NTNU – Trondheim
Norwegian University of
Science and Technology

Silicon Core Optical Fibre Production and Characterisation

An investigation of alkali earth metal oxide interface additives in a fibre production method.

Andrew Dibbs

Condensed Matter Physics
Submission date: June 2013
Supervisor: Ursula Gibson, IFY

Norwegian University of Science and Technology
Department of Physics

"No problem is too small or too trivial if we can really do something about it."

Richard Feynman

NORWEGIAN UNIVERSITY OF SCIENCE AND TECHNOLOGY

Abstract

Department of Physics

Master of Science in Condensed Matter Physics

Silicon Core Optical Fibre Production and Characterisation

by Andrew Dibbs

Solid semiconductor optical fibres are of interest for infrared transmission and guided wave photonics. Transmission of optical fibres in the 2-6 micrometer wavelength region is difficult with today's materials, and the possibility of combining photonic and electronic components in one material has attracted much attention. This thesis presents a method of improving the quality of solid silicon core optical fibres made in a rapid draw process. It does this by the introduction of a alkali earth metal oxide interface modifier between the silica and the silcon core. This modifier acts as an *in situ* oxygen and metallic impurity getter. These investigations indicate that the interface layer forms a eutectic that reduces the stress caused by the expansion of silicon upon freezing. The silicon fibres made with this interface layer have greater mechanical flexibility than those without, but the optical losses are comparable to fibres made by other methods.

Acknowledgements

First and foremost I would like to acknowledge my supervisor, Ursula Gibson and Erlend Nordstrand without whom this thesis would not exist. Their patience with me went beyond the call of duty.

My thanks also go to Fredrik Martinsen for his help in preparing fibres and getting data.

My thanks to the rest of the Silicon working group: Andreas Eraker, Matthew Bohn and Mona Karbaschi.

Finally, I would like to thank G. S. Kanda for his open discussion and frank opinions on style.

Contents

List of Figures

List of Tables

Abbreviations

AFM	**A**tomic **F**orce **M**icroscopy
BSE	**B**ack **S**cattered **E**lectron
COMSET	**C**enter for **O**ptical **M**aterials **S**cience and **E**ngineering **T**echnology
CVD	**C**hemical **V**apour **D**eposition
EDS	**E**nergy **D**ispersive **S**cattering
EPMA	**E**lectron **P**robe **M**icro **A**nalysis
FEPA	**F**ederation of **E**uropean **P**roducers of **A**brasives
HPCFD	**H**igh **P**ressure **C**hemical **F**luid **D**eposition
IC	**I**ntegrated **C**ircuit
ID	**I**nner **D**iameter
mIR	**m**id **I**nfra **R**ed
MRI	**M**agnetic **R**esonance **I**maging
OD	**O**uter **D**iameter
OVD	**O**utside **V**apour **D**eposition
PPB	**P**arts **P**er **B**illion
PV	**P**hoto **V**oltaic
RMS	**R**oot **M**ean **S**quare
SBS	**S**timulated **B**rillouin **S**cattering
SE	**S**econdary **E**lectron
SEM	**S**canning **E**lectron **M**icroscopy

SIMS	**S**econdary**I**on **M**ass **S**pectrometry
SRS	**S**timulated **R**aman **S**cattering
TEOS	**T**etra**e**thyl **O**rtho**s**ilicate
WDS	**W**avelength **D**ispersive **S**cattering
XRD	**X**- **R**ay **D**iffraction
ZBLAN	**Z**rF4- **B**aF2-**L**aF3-**A**lF3-**N**aF

Chapter 1

Introduction

This introduction is an attempt to give a fuller understanding of the historic background, motivation and scope of the material that will be covered in this thesis.

1.1 History and Background

Elemental silicon has not always been in the position of importance in its application and use, that it has today. Originally it was being used only as a "poor man's alloying agent" [1] in the aluminium industry. Almost a century after its first use it found its first application as an electronic material as a rectifier in the second world war. However it was in 1954, when it was first made into a solid state transistor, that it began to truly attract attention and development.

The majority of silicon by mass is still within the production of metallic alloys or as a deoxidising agent. However it can be argued that the greater impact of silicon is within electronic and solar photovoltaic (PV) industry. It is the substrate for integrated chips (ICs) and for making solar panels that generate power directly, rather than through thermal means. These uses require ultra-pure silicon, and hence this has caused the technology and method involved in the production of high quality silicon ingots and boules to increase immeasurably. The working processes required to convert the ingots and boules into the final product have become refined almost beyond recognition from the first few faltering steps.

The silicon fibres discussed in this thesis are called such due to their aspect ratio of a length that can be considered "infinitely" long compared to their circular diameter. (Additionally as their optical nature is of primary concern, although not sole, fibre will be used rather than "wire" to avoid the associations with metallic conductive wire.) In 1966, C. K. Kao suggested that fibres could be used to conduct light at optical frequencies for communications[2]. For this he was awarded the Nobel Prize in Physics in 2009. Kao suggested that if optical losses from the transmission of light could be brought below 20 dB km^{-1} it would bring the concept into the realm of the commercially viable. A 20 dB km^{-1} attenuation would allow 1% of light intensity to be present at the end of a 1 km stretch of fibre. This, he goes on to say, could be achieved by the removal of metal impurities that were endemic throughout fibres at the time (which led to contemporary fibres having a loss significantly greater than this). Unbeknownst to Kao at this time researchers at Corning (D. Keck, R. Mauer, and P. Schultz) were developing a method to improve the quality of silica waveguides. In this process they were able to draw 100 μm silica optic fibre with losses around 16 dB km^{-1} in 1970 as claimed in their patent ('Method of producing optical waveguide fibers', US3711262). This kick started development and implementation of fibre optics as it could carry several orders of magnitude more information than copper electrical cable.

ICs are an integral aspect of computing, are called such as they integrate on a single chip (or wafer) many functions that in the early days of computing were distributed. So far, even though there have been efforts to diversify the geometry of ICs [3] most of the development has been and is ongoing on planar devices, as these represent the most easily implemented and conventional and therefore the most reliably produced. However, with continued miniaturisation and power concerns, growing interest has been directed towards optical computing to continue the increase in computing speed. It can achieve this by taking the burden of switching between optical and electrical signals by performing operations on the light directly. This would free up "real estate" on any conventional IC die that would still have to be used and keeping the benefit of the lower power while retaining the higher speed that using light would bring [4]. Even with different geometries of ICs though, any mechanism that shifts the burden of additional processing will result in the possibility of increasing the total overall. One of the challenges of the realisation of an optical computing solution is the integration of the electrical and optical systems through appropriate interconnects [5].

Similarly, in the field of silicon PV there are efforts at finding novel methods of increasing the efficiency of the modules created. One method by which this can be achieved is by increasing the light capturing properties of the silicon, which is possible when the geometry of the silicon is changed to fibres. This could potentially increase the generated photo-current using the same materials.

Optical power transfer has been suggested for applications where electrical current and the magnetic field they generate is significant enough to interfere with measurements such as MRI [6]. Silicon is able to outperform many alternatives due to its optical damage threshold [7] and IR transparency.

Silicon fibres could have applications in telecommunications opening up bandwidth by accessing previously unused optical frequencies. However, there currently exists effective transmitters of n- and mIR such as the heavy metal fluoride glass, ZrF_4-BaF_2-LaF_3-AlF_3-NaF commonly referred to by its acronym: ZBLAN. Fortunately, due to peculiarities in manufacturing [8] very high quality fibre is difficult and expensive to make which could make alternatives attractive. Areas that have hitherto been problematic, such as IR optical switches, could be possible applications thanks to the robust nature and experience of working with silicon. Sensing probes could also be a field that could benefit, as they are often used in places which have harsh environments where the robustness of silicon would be an advantage.

With this need to open up more bandwidth with higher power in telecommunications and power transmission, sensing a wider range of input in sensors and ability to manipulate light for optical computer, there has been an increase in the importance for lasing sources outside the regions currently exploited, particularly at lengths over 1 μm. As stated before, silicon is an obvious choice as it benefits from the prior experience and development in the technology. Additionally, silicon also has a high index of refraction that increases its wave-guiding properties, allowing a higher density of fibres in close proximity [9]. It also has interesting properties when it comes to non-linear optical response which enables the manipulation of light pulses [4]; consequently it has the possibility to be used in photonic applications.

Currently, there are two developing avenues of approach to creating the silica clad solid silicon core optic fibres: HPCFD (High Pressure Chemical Fluid Deposition) and conventional fibre drawing with silicon in a silica tube preform [10]. HPCFD is a method that has evolved from chemical vapour deposition (CVD). As its name suggests, CVD uses a chemical vapour to transport the desired material and

deposit it via a chemical reaction at the point of deposition. HPCFD, on the other hand, involves using a chemical solution in liquid form at high pressure to transport the desired materials and deposit it where required. In this case this is achieved by applying a high temperature at that point. This allows the fluid to fill cavities with a great enough concentration to enable deposition to take place. As this suggests, it creates the fibres *in situ* and, depending on the fibre type desired as the end result, a high-temperature anneal afterwards. The conventional draw attempts to treat the process in a similar way to the well known and used method of silica optic fibre production, but with a molten core of silicon within the silica preform. Both of these methods have their advantages and disadvantages. For instance, high quality and low loss fibre has been fabricated by Badding et. al. using HPCFD; however, it is deposited in an amorphous state and requires additional processing to obtain a state that returns the properties desired. Additionally, due to the need to transport the fluid through the length of fibre, the maximum length that can be created is limited to around 70 cm [11]. Conversely, Ballato et. al. and Scott et. al., using another method of silicon powder in preform, have created silicon optic fibre directly in a method derived from a conventional fibre draw process, using the same equipment. This provides a lower quality fibre, evident in the shorter whole pieces that are created, although the fibre segments created can be used directly and use technology currently operating for mass production. Consequently, this work has allowed the production of hundreds of meters of silicon fibre [12].

1.2 Motivation, Justification and Scope

The motivation behind this study is derived from the idea that continued use of silicon in the construction of computers and solar PV suggests that silicon will remain an important material for significant period of time. In order to improve on the quality, range and depth of applications for which silicon can be used, this calls for an improvement in some of the current manufacturing techniques. It was noted in [9] that it is believed that one way to open up new commercial applications is via new geometries of silicon. The new geometries have previously been difficult to achieve or have been overlooked. This will can lead to extremely rapid development process as it reaches technological parity.

Progress has been made in the production of high quality silicon fibres that allows unbroken solid lengths to be made, specifically in the conventional draw method as mentioned in previous section. In a report by Ballato [13] he states that oxygen

precipitated in the silicon core during this method could be a source of optical losses. Another study has shown that excess oxygen can cause the creation of compounds that cause fractures on the interface which increases the stress on both silica cladding and silicon core [14]. A better quality fibre could be made with the addition of a suitable compound which can capture excess oxygen while forming a eutectic layer that will remain liquid as the silicon freezes, absorbing the expansion.

Taking the above into consideration, it follows that there are restrictions placed on this compound, viz:

1. Captures excess oxygen by being less electronegative than silicon
2. Forms a eutectic with silicon that is below softening point of silica

In looking for a compound that satisfies these criteria, it pays to look at what is usually used to purify silicon and hence remove oxygen. This leads to the alkali earth metals of which magnesium (Mg), calcium (Ca), strontium (Sr) can be said to "safely" satisfy the requirements [15–17].

This thesis discusses the application, development and the structure of different interfacial layer types between the silicon and silica concentrating on those based on CaO. It will attempt to qualify the effects on the body of the silicon core due to these different types. We will present results on the chemistry and microstructure of the fibre pulled using these modifiers.

Chapter 2

Background

This chapter aims to provide a theoretical understanding for the correct interpretation of the results. It will cover recently investigated concepts in other areas more thoroughly than in the background to provide a more general picture in contemporary research.

2.1 Conventional optic fibre production

This section covers the production of a conventional optical fibre that is currently used in, for example, sensors and telecommunications around the world. Fig. 2.1 shows a schematic of a conventional fibre draw process.

2.1.1 Preform fabrication

The process, mentioned in 1, developed by D. Keck, R. Mauer, and P. Schultz at Corning was the Outside Vapour-phase Deposition (OVD) method. This has, along with others, become one of the main methods of creating the silica preforms. Most of the commonly used commercial methods can be grouped under family of methods called Vapour-phase Oxidation. This commonly uses 2.1.

$$SiCl_4(g) + O_2(g) \rightarrow SiO_2(s) + 2Cl(g) \tag{2.1}$$

The reactants are passed through a tube which is then heated, the temperature causing the $SiCl_4$ to react with the oxygen, forming small particles of SiO_2 which adhere to the side of the tube. The tube is rotated as this happens to form an even layer. The "soot" builds up successive layers of silica leaving a highly pure silica rod. It is possible to dope by using different reactants, thus changing the refractive index. Different preforms can be created this way as different sized tubes, which can then be bonded together to form a larger preform. This is necessary for making stepped or graded index fibre (that is a fibre that has a different or multiple refractive indices). The growing is complete when the silica preform reaches between 20-300 mm diameter and up to 1 m long [18].

2.1.2 Draw process

The preform has a suitable "handle" attached to the end to maximise the proportion of preform used and avoid contamination. It is then placed into a furnace which is then heated to between 1900° and 2200°C. At this point the silica will become fluid enough to start stretching under its own weight. When this initial drop has stretched far enough, the mass at the end is stopped and the heat is turned off. The bulk at the end is cut off where the fibre is small enough for threading through a set of rollers. The rollers enable the pulling force to be changed smoothly while not allowing any slack to develop. The rest of the equipment consists of a laser measuring system, polymer coater and UV curing stages. Then the preform is heated up again, and when it has reached the correct temperature the rollers start pulling the fibre down and the result is spooled on the end reel. While this is still a batch process, due to the difference in dimensions of fibre and preform and the conservation of mass, hundreds of kilometers of fibre can be drawn off a single preform. The fibres that are created in this method tend to have more hydroxyl ions within them, which causes more absorption at longer wavelengths (towards the IR) and as such, there is a separate method which is employed when specifically optimising silica fibres for nIR transmission.

2.1.3 Fibre losses

Losses in fibres are measured in units of decibels (dB) as the power loss is exponential with distance. That is, the rate at which power decreases can be represented by a exponential coefficient. $P(x) = P(0)\exp(-\alpha x)$ where α is the attenuation

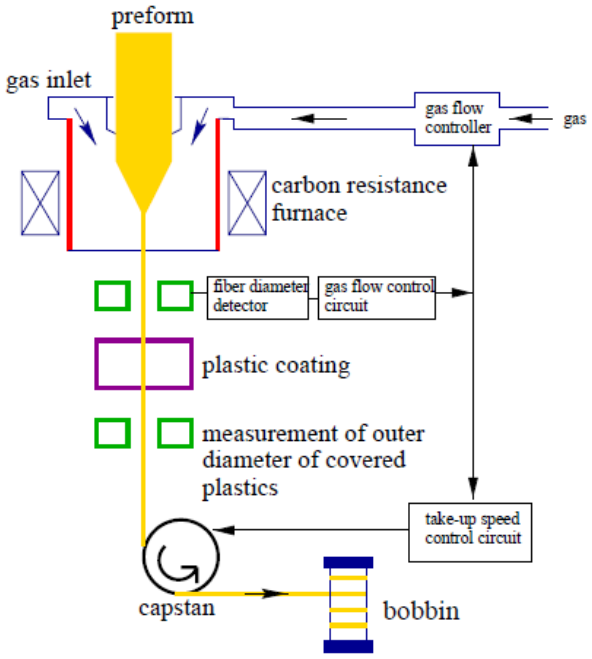

FIGURE 2.1: Schematic of the molten core method [19].

coefficient and so: $\alpha = \frac{1}{x}\ln(\frac{P(0)}{P(x)})$. The attenuation coefficient α is a constant that embodies different sources of loss through the fibre. These losses in occur through a number of different mechanisms. Some of these mechanisms will be covered below, along with the methods used to minimise them. Only losses in the transmission of light will be considered, and not those in coupling it into the fibre.

2.1.3.1 Microbending

Microbending losses occur when a large force has been exerted on the surface of the fibre. This force can cause a small deformation or series of deformations (Fig. 2.2b) of the interface between cladding which provides a scattering object to light. Often, there is nothing that can really be done to correct any microbending damage, hence prevention is best. This can be achieved by knowing the limits of the fibre that is being produced an also by the application of suitable coatings that can absorb stress that builds up [20].

Microbending can come about either by impurities in the fibre or a large external pressure being applied on a small region. When considering microbends they are approximated to a grouping of very small radius bends. Microbends once imposed upon a fibre can often become permanent, as it involves high localised stress and is highly dependent on the fibre conditions properties at that particular point [21].

2.1.3.2 Macrobending

Even when a fibre is bent slightly, there are losses due to the core deviating from a straight line. This results in the light that is travelling down the fibre coming into contact with the edge When the fibre is bent, it changes the incident angle of the transmitted beam with the interface of the core and cladding. If the curvature becomes too great, the incident angle will be above the critical angle, leading to light escaping. This problem is more apparent in multimode fibres, as there are already modes that have a high angle and any change could increase it just enough to put it over. Alternatively, by considering the light propagation as a distribution of its electric field component as in Figure 2.2a. This illustrates that it extends a finite distance into the cladding and when fibre bends it results in the field extending further on one side into free space. When this occurs it results in a loss, which varies depending on how far out it does. Therefore to reduce the losses from macrobending, the only way to minimise it is to not bend it as much as possible. When bending is essential, it is necessary to keep the curvature of the bends to a reasonable distance.

Macrobending increases the attenuation across the spectrum, starting from the longer wavelengths. On the other hand, microbending impacts on longer wavelengths less as the size of the bends is so much smaller than the wavelengths considered and smaller wavelengths propagate over the surface of them.

2.1.3.3 Scattering

All the following different forms of scattering and absorption can occur, which all contribute to the total loss experienced by the transmitted light. Losses accrue via absorption from impurities, Rayleigh scattering and Mie scattering.

Mie scattering is the scattering of light off objects that are on the same order or larger than the wavelength of light impinging on it. They can occur due to

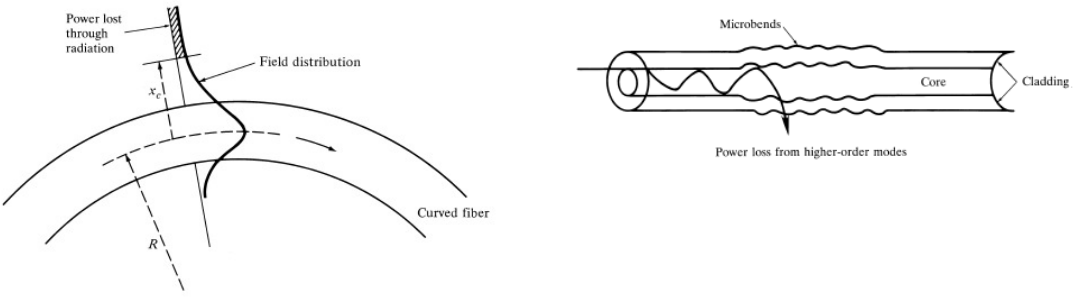

(A) Macrobending (B) Microbending

FIGURE 2.2: Bending losses [22].

the composition of silica changing, including a large change in the density that might come about in the drawing process. Microbending can be a source of Mie scattering along with imperfections that arise from the dynamic nature of the draw and amorphous silica state.

To reduce the number of Mie scattering objects in the fibre, and thereby reduce the attenuation undergone by light, the draw can be performed in a clean environment in an inert atmosphere. Carefully controlling the pull by varying speed as slowly as possible while maintaining diameter restrictions can also help. As in the microbending case, coatings are good at protecting against any development of such scattering objects, as they drastically reduce impurities coming into contact with the cladding [22].

Rayleigh scattering is due to localised particles that are smaller than the wavelength of light or a small scale variation of refractive index due to a change in density. This can arise from a few sources such as molecules that have been intentionally used to dope the fibre. This also includes the oxides that form the glass themselves, which means that Rayleigh scattering is an intrinsic property and not much can be done specifically for it [23].

There are also non-linear scattering processes that can arise in optical transmission through a medium. When the optical power output of the fibre (in this case) is not directly proportional to the input, there is said to be non-linear scattering. Compared to the previous scattering types above which are elastic events, non-linear scattering is inelastic. That is, Rayleigh scattering doesn't change the energy, just the angle (although it tends to be in a forward direction): the energy between the

scattered light and incident light is not the same. In non-linear scattering, this is not the case [24].

There are two interactions that are the most significant: Stimulated Raman scattering (SRS) and Stimulated Brillouin scattering (SBS). These two differ in the type of phonon that interacts with the photon. SRS interacts with an optical phonon, and SBS an acoustic. The processes are largely similar: A photon is absorbed by a molecule, which excites an electron. The electron will then de-excite dropping to a lower energy level with the release of a phonon. Conventionally, the energy difference is the same as the energy of the incoming photon. However, it is possible for transitions to occur where the electron jumps to a higher energy level, resulting in a lower energy photon being emitted: a Stokes-Raman scattering event. Conversely, it is also possible that the electron will fall to a lower energy level which emits a higher energy photon: an anti-Stokes-Raman scattering event[22].

Usually this scattering is to be avoided as it causes disproportionate attenuation at desired wavelengths, however there are a few instances where it is desirable, such as in photonics. The emitted photons are of lower and shorter wavelength respectively. This change in wavelength results in an attenuation of the desired information carrying wave packet.

Nonlinearity in fibres arises from the thermal vibrations through the body of the fibre and to minimise its effects requires keeping the optical power density down. The effects on the signal can be used to deduce different kinds of material properties of the fibre.

2.1.3.4 Absorption

The difference between absorption and scattering is that when the light is absorbed it is not scattered again in any usable form, instead the energy is used to excite the molecule or atom's vibrational mode rather than that of an electron. Table 2.1 gives a quick comparison of different commonly found impurities and the attenuation caused at a fixed concentration. The effect of the hydroxyl group (OH-) is even greater as it has multiple absorption peaks at 2700, 1400, 960 and 725 nm and tends to be stronger absorption. In fact, if less than 20 dB km^{-1} is to be reached there has to be less than a few parts per billion (ppb) which in comparison to the metal ions in 2.1 is a lot more.

TABLE 2.1: Comparison of the absorption wavelengths and extent that common metal impurities have on silica optical fibres. Adapted from [22]

Impurity	Peak wavelength (nm)	One part in 10^9 (dB km^{-1})
Cr^{3+}	625	1.6
C^{2+}	685	0.1
Cu^{2+}	850	1.1
Fe^{2+}	1100	0.68
Fe^{3+}	400	0.15
Ni^{2+}	650	0.1
Mn^{3+}	460	0.2
V^{4+}	725	2.7
OH^-	950	1.0
OH^-	1240	2.0
OH^-	1380	4.0

Clearly, to minimise losses of this nature, it is necessary to reduce the impurity content of any fibre to as low a value as possible.

2.1.3.5 Dispersion

Any distortion, a change from what was put into the fibre, of the light signal can be considered dispersion. As it occurs in all mediums through which light passes a certain amount is to be expected; however once a certain degree of dispersion is reached, it is unable to reconstruct the original signal. The rate at which this occurs is usually nanoseconds per kilometer and should be minimised.

- Chromatic dispersion or Intramodal is dispersion within a single transmitted mode which comes about due to the finite spectral line width of the optical source. This simply means that the pulse that is sent is composed of slightly different frequencies. These frequencies may be delayed slightly due to the materials' tendency to propagate different frequencies at different speeds.
- Mode dispersion, also called Intermodal arises from the differences between separate modes. This does not exist in a single mode fibre which is one of the reasons there is significantly less dispersion in the signal using a single mode fibre. Graded fibres are better than step index fibres in this as well.

2.2 Solid silicon core optical fibres

There are a couple of methods to produce solid core optic fibres which do not involve intermediary chemical transport and can be applied to current commercial methods. By varying the fibre pull speed, in both the above method and when attempting to fabricate a solid core silicon fibre, it is possible to create thinner or thicker optic fibres that may be required for different purposes.

2.2.1 Previous work

As mentioned in Chapter 1 there are a few people working on creating solid core optical fibres, of these there are two which have a draw process that is similar to the process developed in the works that have contributed to this thesis.

2.2.1.1 Molten core

The molten core method is used by Ballato et. al. at the Centre for Optical Materials Science and Engineering Technologies (COMSET) at Clemson University in South Carolina in the United States. In this method, they create a large tube from concentric telecommunication purity silica tubes so they fit inside each other leaving an outer diameter of ≈50 mm and an inner diameter of 3.5 mm [13]. The tube is sealed by fusing another solid piece of silica on to one of the open ends. The draw took place at around $1950°C$. The silicon that was used was a rod that was drilled from a Czochralski monocrystalline boule.

Initially the fibres that were pulled were drawn at 2.7 m min^{-1} were thick between 1 - 2 mm O.D. and 60 - 120 μm I.D (inner core diameter). At this thickness, there was very little flexibility in them [13]. The lengths of unbroken and large defect free silicon core in the fibre were around 5 cm. It was found that there was a very high purity of silicon in a polycrystalline state. This was verified by an X-ray diffraction (XRD)test and the Raman spectra of the Si core by comparing it with a known ultra high purity, monocrystalline sample. There was a high correlation between the XRD from a single crystal and the core of the silicon fibre. The amount of SRS that occurred was also very similar, suggesting large crystal grains. For SRS this is due to the phonons that are involved in SRS, similar phonon environment must be involved and they are usually scattered at grain boundaries.

The loss in the fibre was determined to be around 4.3 dB m^{-1} using a wavelength of 2.936 μm. It was found that there was quite high oxygen content of 17% across the silicon core. This could have caused some of the scattering and attenuation by causing precipitates of stable SiO_2 to form on cooling.

Due to the high quantity of oxygen they found in the core of the fibre, a method of reducing it was developed. This method was the addition of a quantity of silicon carbide (SiC) to the core silicon, which acted as a getter of oxygen. The SiC reacts with the SiO_2 precipitate to form Si, SiO and CO. SiO and CO are both gases which can then be removed. This was used and found to reduce the oxygen content dramatically. However, while this reduced scattering this did not improve the overall losses that were measured at 1-3 μm, 9.7 dB cm^{-1}.

The longest crystal grains were shown to be in the [1 0 0] and [1 1 0] directions, also from an XRD study. The grain boundaries were very complex and no parameters could be determined from them. The surface of the silicon core was generally very smooth with only peaks up to 25 nm above the surface and an root mean squared (rms) of less than 4 nm. To try and improve the crystallinity of the fibres that were pulled, they pulled them so they used another heater and applied extra strain to stretch the fibres up to a certain degree forming a tapered fibre [25].

2.2.1.2 Powder-in-tube

Scott et. al. in Refs. Powder, FabofNtype, GrainsizeDiameter created a fibre by first making a tube with an O.D. of 6 mm, I.D. of 3 mm they then sealed one end of the tube and filled it with a powdered silicon. The silicon used was composed of n-type wafers ground down in a silica pestle and mortar.

The drawing machine is composed of two chucks that are mounted on two lathes that can be accurately spun separately or together and then one of them can slide along a rail. When the preform is clamped in the the chucks, the tube is heated via a oxygen-hydrogen burner. The preform is spun while heated to provide uniform heating over the tube. When the desired temperature has been reached, one of the chucks slides back, drawing a fibre. While the preform is being heated, a vacuum is applied to the end, removing air and any gases that are produced.

The silicon core fibres that were made ranged between 10 and 100 μm in diameter and 7 cm in length. In measuring the optical losses at 1.52 and 1.57 μm, it was found that the end face of the fibre greatly affected creating up to an additional

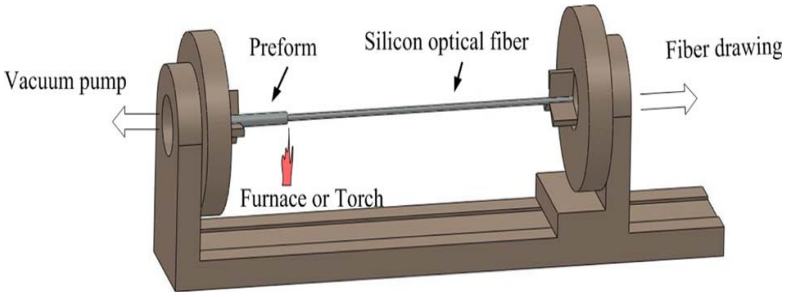

FIGURE 2.3: Schematic of the powder-in-tube method [26].

15 dB of loss. Overall loss was found to be approximately between 4 and 5.57 dB cm^{-1}

2.3 Properties

2.3.1 Silicon

Silicon is a Group 14 (traditionally called Group IV) element, some of its properties have been listed for comparison with silica in Table 2.2.

The viscosity of silicon up to 1800°C varies in a linear fashion between ≈ 0.532 and 0.576 mPa s while in a quartz crucible [27]. More importantly, like water it has a positive thermal expansion coefficient of $\approx 9\%$ upon freezing [28]. This causes many of the problems in the creation of optical fibres as when it freezes, it expands out, applying stress to the quartz cladding. Strain increases with decreasing surface area, however this is dependent on surface flaws [29].

In this case the silicon core could be a range of crystallinity which also affects the strength. If the crystal is monocrystalline, depending on the orientation, it can withstand greater stress so certain directions may be stronger. Although there is a very low chance of creating a mono-crystalline fibre structure for a number of reasons: the rapid rate of cooling freezes the orientations of the developing crystal into whichever form is locally favourable; the variable interface with the eutectic changes these conditions over a range; and the uneven draw speed changes the amount of silicon that will be freezing at any given time, which is changing the coating to silicon ratio. It has also been noted in Ref. [30] that circular core waveguides are less likely to crystallise into a mono-crystalline structure than square.

Torsional forces will also increase the chances within a crystalline structure. At grain boundaries there are weaknesses: microfractures in the silicon, which could be formed from previous bending, exposure to air or water or just from the cooling process.

TABLE 2.2: Properties of Silicon and Silica [31, 32].

	Silicon	**Fused Silica**
Mechanical strength		
Density, (g cm^{-3})	2.33	2.2
Youngs modulus, (GPa)	158	72
Fracture toughness, (MPa $m^{\frac{1}{2}}$)	3-6	0.79
Thermal properties		
Melting point, (°C)	≈1414	≈1830[a]
Viscosity after melting/softening, (Pa s)	0.532×10^{-3}	8.3×10^{-6}
Thermal Conductivity, (W m^{-1} K^{-1})	156	1.45
Coefficient of thermal expansion, ($°C^{-1}$	2.6×10^{-6})	5.5×10^{-7}
Optical Properties		
Index of Refraction	1.54	1.46[b]
Attenuation coefficient	see Figure 2.4	

[a]Although it softens at a lower temperature ≈1680
[b]In the range that it would be under consideration, it only decreases.

2.3.2 Silica

Silica often goes by other names such as silicon dioxide, SiO_2, fused quartz and slightly incorrectly as quartz. Quartz is slightly erroneous as it has a crystal structure while having the same composition.

As shown above in Table 2.2, silica softens over a broad range from 1600° to 2300°C progressively becoming more and more fluid. This makes the fibre making process strongly dependent on temperature. The viscosity of silica at its softening point is 8.3×10^6 Pa s.

While the stress required to fracture bulk glass can be relatively low, at around 100 MPa, this is orders of magnitude lower than for the force required to break the bonds within silica, which would be approximately 10,000 MPa. Consequently if a silica tube has a breaking stress of 2.37 MPa theoretically it can be as low as 0.17 MPa in practice [33]. Therefore the quality of the fibre that is created not only

has an impact on the optical transmission of a fibre, but also on the amount of stress that it can withstand before breaking. The breaking stress is also influenced by cristobalite growth. This is exacerbated in the presence of water which, as a hydroxyl compound is being used, is present in the heating of $Ca(OH)_2$ [34], which results in the the glass often becoming very fragile.

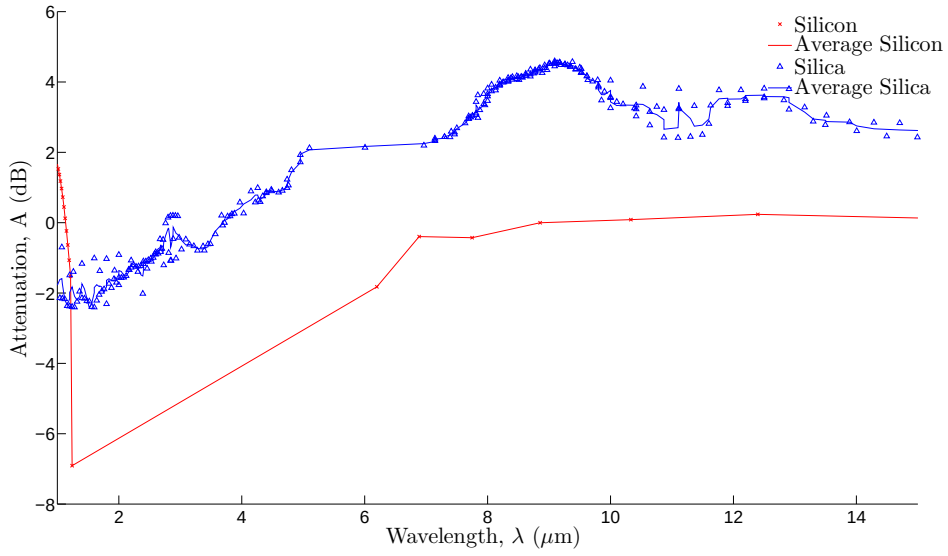

FIGURE 2.4: The attenuation of silicon against that of silica in across the wavelengths on interest. Combined data from multiple sources. Data is from [35, 36].

2.3.3 Alkali earth metals and their oxides

As their group name suggests, these compounds are basic to varying degrees. All of them are mainly found in an oxidised state, whether as their monoxide or in carbonate form. Their name "earth" is derived from the fact that their oxide states have such a high melting point that they remain solid in fires. Table 2.3 shows a comparison of various relevant properties of the oxides in question.

TABLE 2.3: Properties of Alkali earth metal oxides and hydroxides [37]. Density is rounded to 2 decimal places and solubility is in water at 20 °C.

	Density, (g cm^{-3})	Melting point, (°C)	Solubility, (g (100 ml)$^{-1}$)
CaO	3.34	2613	Reacts
$Ca(OH)_2$	2.21	580	0.173
MgO	3.58	2852	Reacts
$Mg(OH)_2$	2.34	350	0.0014
SrO	3.74	1494	0.0011
$SrCO_3$	4.70	2531	Reacts

2.4 Eutectic solidification

A eutectic system is one where the combined melting point for a mixture of two or more materials is lower than for the individual constituents. This phenomenon has been used for many centuries to solve numerous engineering problems. Traditionally it is when two metals are mixed in a specific ratio which results in an alloy with a lower melting point. This allowed the development of materials that supply increased overall performance (i.e. strength and durability) [38]. The eutectic point is the region where the lowest temperature can be achieved while all phases are in a liquid state. This occurs at specific molar concentration ratios between the components. If these ratios are not met, there will be a gradual solidification whereby the excess material will precipitate out of the solution progressively until the liquid solution contains the proportions of the eutectic point. When this happens, there is a sudden simultaneous crystallisation by all phases.

Eutectic structures are not formed only with metallic components. Systems that contain eutectics enable the creation of many different alloys with properties similar to those of materials that would be more difficult to work [39]. Regardless of the materials that are associated with the eutectic, the process remains largely the same. While in its liquid phase, the mixture is considered a homogeneous mix of all the components, being subject to the dominant thermal actions and diffusive effects. When the solution cools beyond the eutectic point the different components begin to precipitate out of the solution simultaneously. Depending on the properties of the materials involved, they will do this in different ways, for example in what is characterised as "Normal Eutectic Growth" there will be simultaneous growth in one front by both components, leading to a clear front. The regions formed are flat planar alternating between either. The driving force

behind the crystallisation is the undercooling that occurs, hence the crystallisation front travels in along the direction of the heat flow upon cooling [38].

Some of the factors that influence the growth and determine what kind of growth is exhibited are:

- Volume fraction of materials.
- Entropy of melting and fusion.
- Diffusion constant of components
- Rate of cooling.

These factors cover numerous other factors that are outside the scope of this thesis. However it should be known that changing these factors can change the expression of the eutectic solidification. This could alter the properties of the drawn fibre. Following are phase diagrams for the systems that will be produced in the fibres.

In this thesis these oxides are combined with water forming hydroxides. Consequently, taking into consideration how the hydroxides behave is important. It is found that the decomposition of $Mg(OH)_2$ can begin at a low temperature (e.g. around 250°C), but proceeds a lot quicker at higher temperatures [40]. The decomposition of $Ca(OH)_2$ into CaO occurs at ≈512 °C [41] and $Sr(OH)_2$ decomposes around 375 °C [42]. As such it will be assumed that upon heating, up to the melting point of silicon at the very least, these compounds will be converted back to their oxide form. Therefore the following diagrams involve only the MO_x form where M is the alkali earth metal.

Ref. [46] puts forward that there is only a stable phase line between MgO and Si, meaning that MgO will not react with Si so there will be no change in phase. This is supported by Ref. [47] along with FactSage calculations, although there is disagreement with temperature values in the SrO-SiO_2 system.

This shows that as eutectic mixture will be present in the fibre. Although in some cases, there are quite complex processes going on, it is unclear what exactly will happen. There is a stable line from MgO to Si in 2.6a this represents the fact that silicon cannot take the oxygen from the magnesium oxide. This is related to the strength of the bond between the alkali earth metal and oxygen which derives from its electronegativity. The electronegativity is the measure of how much an atom attracts other electrons to it and in general decreases as the atomic number

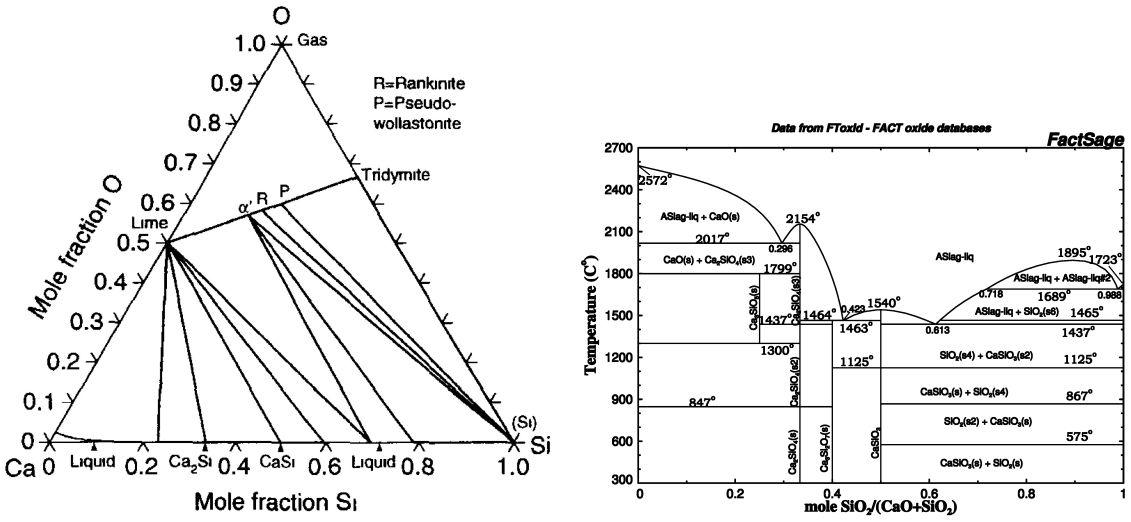

(A) Ca-Si -O system at 1500 °C [43]. (B) CaO - SiO_2 system [44].

FIGURE 2.5: Phase Diagrams for CaO with Si and SiO_2

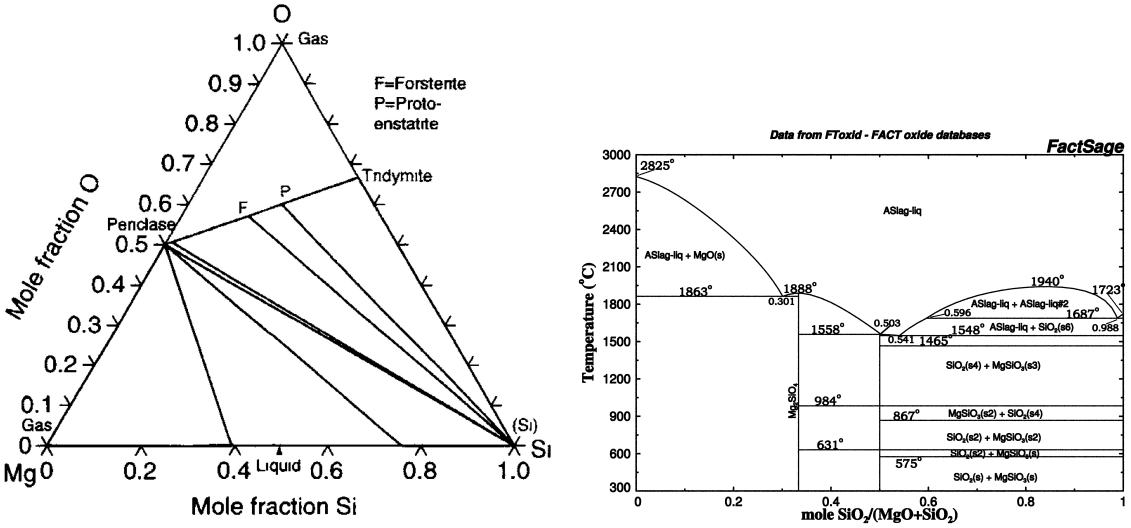

(A) Mg-Si-O at 1400 °C system [43]. (B) MgO-SiO_2 system [44].

FIGURE 2.6: Phase Diagrams for MgO with Si and SiO2

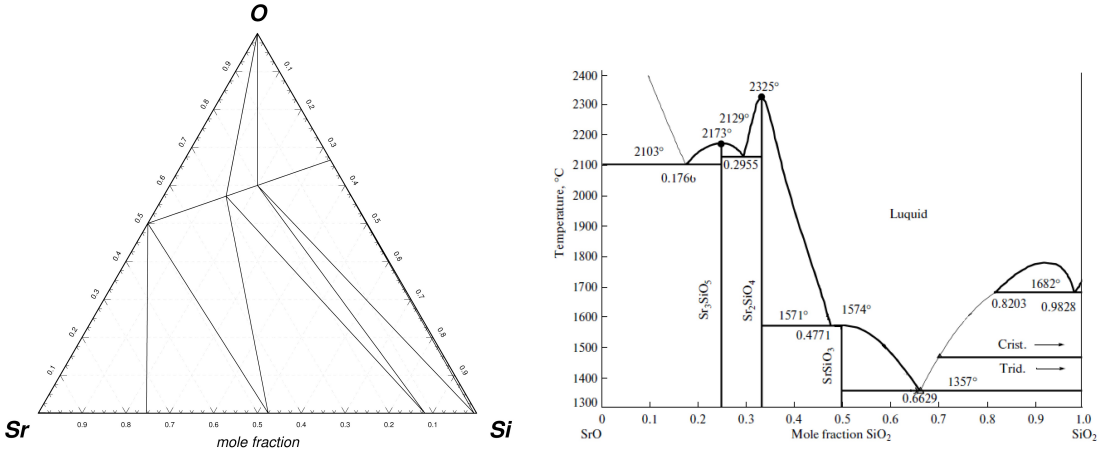

(A) SrO-Si system (B) SrO-SiO_2 system [45].

FIGURE 2.7: Phase Diagrams for SrO with Si and SiO2

increases. Hence, magnesium which is more massive than calcium has a lower atomic number has a higher electronegativitiy, is more tightly bound with oxygen and does not dissociate as easily in the presence of another electronegative atom: Silicon.

2.5 Characterisation methods

Some of the characterisation methods that have been used are described below.

2.5.1 Bending radii

Bending radius is the most curvature that a fibre can undergo before experiencing permanent damage. This could mean either that the fibre suffers a catastrophic break, severing it entirely, or that small interior fractures and surface deformations are induced: both cause interference and degradation to the carried signal. If there is already damage within the fibre and it is subsequently bent, the fibre carries a greater risk of snapping entirely. Corning test silica fibres to 100 kpsi (689.48 MPa) and recommend limiting stress to one fifth of that to reduce the risk of damage. However that is for silica glass and so has a different strength [21] however the principle is the same.

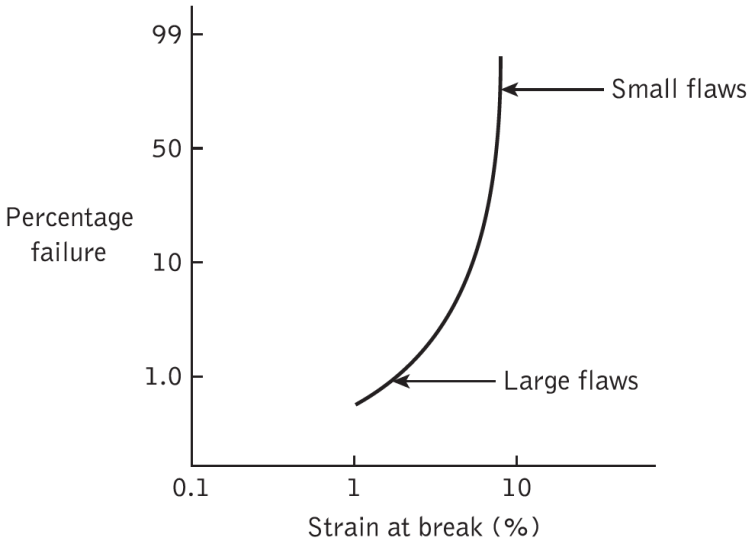

FIGURE 2.8: The strength of a fibre is dependent on the flaws that are within the fibre. Larger defects can break the fibre at lower strains, however there is less space for bigger flaws and hence a lower probability of it occurring. Figure is from [48] regarding silica optical fibres.

2.5.2 Void count

The number of voids that are present in an arbitrary cross section of the fibre gives an indication on the quality of the silicon bulk.

2.5.3 Scanning Electron Microscope (SEM)

A scanning electron microscope works by accelerating electrons from an electron source. The electrons are focussed onto a sample which scatters the electrons. The electrons are picked up by a detector and used to form an image of the surface. As electrons have a mass, they can be expressed as having a de Broglie wavelength. This wavelength is a lot smaller than optical photons which means that their resolving power is greater. Although, unlike an optical microscope it does not depend on the focussing of the scattered particles, but the size of the impinging beam. As such it can be used to study very small objects down to a matter of nanometers. It is these secondary electrons (SE), that is the electrons that are

ejected from their orbits by the incoming beam, that are most commonly used to form an image; however, it is also possible to use the backscattered primary electrons (BSE). The BSEs are the result of elastic scattering with the sample, and as such they embody significantly more energy than SEs. This provides an easy way of differentiating them. BSEs give a different set of information than SEs. As the electrons have been scattered 180° (taking 0° is in the initial direction of travel) it means that it has experienced an impact that must be within a certain angle for it to be captured by the detector. As electrons scatter from other electrons, the probability of them scattering is greater when hitting a greater concentration of them, which is around higher atomic number atoms. This effectively means that it gives a compositional view of the sample. On the other hand, SE images show the topographical in more detail.

2.5.4 Energy Dispersive Scattering analysis (EDS)

EDS is the measurement of the X-rays that are emitted from the object under study when subjected to high energy electrons. When the electron strikes an atom of the object, it excites an electron from it to an outer shell. This electron will then dissipate the excess energy in the form of an release of electromagnetic radiation with the same energy as the gap between energy levels. There is a finite number of energy jumps that are possible for one atom and this combination of energies is unique to that particular atom and are called the characteristic X-rays. The concept of bombarding a sample with electrons is not new and is used in a SEM; as such they are often combined. Measurements of this kind in this thesis are carried out on a Hitatchi TM3000 tabletop SEM.

2.5.5 Electron Probe Micro - Analysis (EPMA)

The microprobe that performs the scans operates on the same principle as the SEM; however instead of EDS, it uses wavelength dispersive scattering (WDS). This differs from EDS in that separate wavelengths of the characteristic x-rays that are created are analysed one after the other to build up an image of the elemental composition. The wavelengths are selected using Bragg reflection through an analytical crystal Measurements from the EPMA were made using and acceleration voltage of 10 kV and probe current of 5.155 nA.

Table 2.4: Comparison of the characteristics of both EDS and WDS [49, 50].

WDS	EDS
Higher spectral resolution	Lower spectral resolution
Slower data collection	Faster data collection
Lower detection limits	Higher detection limits
Sensitive to geometry of sample	Less sensitivity to geometry of sample
Less spectral artefacts	Spectral artefacts
Moving mechanical parts	No moving mechanical parts
Relatively high beam current typical	Lower beam current feasible
Great for majors and traces	Great for majors, poor for traces
Very expensive	Less expensive to purchase
Larger spacial resolution (≈200 nm)	Smaller spacial resolution (≈5 nm)

2.5.6 Secondary Ion Mass Spectrometry (SIMS)

SIMS works on a different principle entirely. It is a small scale destructive sampling technique. That is, a small area is chosen, and that area will be destroyed during sampling. A molecule (often an elemental gas molecule) is ionised, and accelerated. The ion is guided towards the sample and targeted at the sample. When the ion collides, it can ionise and knock out one of the constituent molecules. These secondary ions are collected and mass spectrometry is performed on them. They are then separated by their charge-mass ratio. The data gathered allows the identification of the ejected ions and thus the sample. Through this method it is possible to resolve elements down to parts per billion.

2.5.7 Atomic Force Microscopy (AFM)

Among the highest resolution of microscopy, AFM can resolve features down to atomic scale [51]. It achieves this by exploiting the force that arises when atoms come close to each other by bringing the tip of a probe very close to the surface of a sample and measuring the difference that occurs due to the interaction of these forces. There are two general types of AFM that are in operation: contact or non-contact [52], although there does exist hybrid modes which operate between the two. Broadly speaking in contact mode, as the name suggests, the tip comes into "contact" with the material; that is the tip experiences the electrostatic repulsion of electrons between tip and sample, and the tip is then dragged across the surface with the change in height being measured. In non-contact, the tip is oscillated

above the surface about 50-150 Å(= 10^{-10} m), at this distance, Van der Waals forces dominate. This is where in the vast majority of cases atoms react as small dipoles and attract one another [52]. The amount of this attraction depends on the distance between them, and this changes the energy required to keep the probe oscillating at the same frequency thus the distance can be calculated.

2.6 This work

As stated, it is hoped that whichever interface modifier is used will be able to form a eutectic layer between the silica and silicon to relieve the stress that develops via the expansion upon freezing. it is hypothesised that this layer will capture excess oxygen preventing its infiltration into the bulk of the silicon core. It could also provide a sink for additional impurities [17].

Chapter 3

Method

This chapter covers the sourcing of the materials used as well as the method used in the production of the silicon fibres. It will provide an understanding for any particulars in the results that follow.

3.1 Sourcing

3.1.1 Tubes

A variety of different tubes were used in the course of these experiments. In-house tubes are from those commercially available and were pure silica with 4 mm O.D. 2 mm I.D and 5 mm O.D, 3 mm I.D. Custom made tubes were obtained from Clemson when solid cores were made. From the sizes of cores that were able to be made and the approximate thickness of coatings, the solid core fit very well in slightly larger tubes.

It was hypothesised that as the viscosity difference between the molten silicon and glass was so great that it was limiting the ability to successfully pull fibres. To test this, a brief experiment with Vycor (a glass with a lower melting point and therefore lower viscosity) was conducted. In it, the exact same "standard" procedure that is laid out below was used, substituting in a Vycor tube. Unfortunately, this resulted in the tube melting far too early and melting away before the silicon could form a stable melt region.

For the most part of the experiments to follow, the smaller 4:2 mm tubes were used as it was possible to control the temperature more effectively with the flame.

3.1.2 Materials

There were a couple of sources of silicon available, E6 and n-type wafers from NORSUN with a purity of 7Ns that is 99.99999% pure. The silicon that was used was prepared as a powder in a mortar an pestle to $\leq$5 mm and solid cores. To create the silicon cores, silicon was loaded into a graphite crucible and then put into an induction furnace. A low vacuum was formed and then argon was flushed through to create an inert atmosphere. Silicon was then melted. A quartz tube was lowered into the melt and the silicon drawn up rapidly where it solidified quickly. It was then possible to retrieve some of the silicon core by breaking the quartz coating at the end which was in the melt, as this was hotter and bonded to the silicon. These cores could then be used in the drawing of fibres.

The CaO, $Mg(OH)_2$, $SrCO_3$ purities were all $\geq$99.9% in powder form.

3.2 Slides

To study the coating more conveniently, microscope slides were used so the coating could be studied more easily. The samples were standardised by depositing the same quantity of coating into the same surface area of slide. This was achieved by punching a standard hole into paper of a fixed size and depth. The paper was then placed onto a glass microscope slide creating a small well. The volume was calculated so just enough coating was deposited in the shallow cylinder. This was done to create the same environment for the slurry enabling a direct comparison to be made. and allowed to dry for 12 hours and assessed under a microscope.

It was initially found that paper tended to wick the water away from the sample rapidly; however, as water content is a parameter of interest, silicone was also used in place of paper so it was retained in the slurry. This gave extra information on how the slurry dried.

3.3 Fibre Method

From earlier testing it seemed that it would be most effective in producing fibres using calcium oxide and binary mixtures of it. Hence the following is the process undertaken when drawing and studying the fibres in this thesis. We will be adapting the method that was developed by Scott et. al. the so called "powder-in-tube" method [26, 53].

3.3.1 Oxide preparation

Making the oxide slurries initially required the establishing of the best ratio of water to oxide. This was achieved for each oxide by slowly adding water to a quantity of oxide. However, this was not as simple as hoped, at least for the CaO, as the quantity of water added was liable to change. A ratio of about 3:1 water to CaO was found to work quite well, allowing for any variation and being able to compensate for many irregularities at a later stage. For water to magnesium hydroxide a 1:1.15 ratio worked quite well and the same for strontium carbonate. However, strontium carbonate did not create a smooth slurry, but rather clumps together and is quite granular.

A capillary glass tube was also used by sleeving it on the inside of the main tube. The capillary is made of a special glass composed of sodium and calcium oxides formed incredibly thin (0.001 μm)

3.3.2 Coating

The coating was performed by drawing the liquid mixture up through the tube with the aid of a vacuum chamber. The end of the tube was placed in the slurry, and the other end was connected to another tube which passed into the vacuum chamber. Within the chamber, the tube ended in a beaker to catch any of the slurry that was passed all the way through. To create a fairly homogeneous coating, the slurry was drawn through with around a 300 mbar vacuum in the chamber. This was dependent on the viscosity of the slurry, which especially in the case of CaO, could vary significantly. Once coated, the tubes were then placed in a drying cabinet at 100°C overnight which equated to at least an eight hour period. The tubes were then weighed again and sealed. In the case of the capillary coating, it

was possible to just slide in the capillary as far as it would go, very lightly score a mark where it extended beyond the preform. Following this, the end was put into a bag and a little pressure applied. The end easily either snaps off or fragments energetically.

The coating was calculated to be roughly around the levels stated above by taking measurements of the mass of the tube before and after the coating process and calculating the thickness that would be produced by that amount of mass of oxide. This was checked by looking at a coated tube under a microscope (Appendix A.1). This was also calculate to give an approximate ratio between the coating and silicon around 1:8 by weight respectively.

3.3.3 Tube loading

The silicon was prepared either by using premade silicon cores, or by grinding large chunks or wafers in an alumina crucible that was cleaned with ethanol thoroughly beforehand. Loading the tubes was carried out by funneling silicon powder into a set of tubes of decreasing size, which terminated with a tight seal around the tube. This was gently shaken until the tube was full. The silicon was a mixture of powder and fine grains no bigger than 0.3 mm.

3.3.4 Fibre pulling

A oxyacetylene torch was used to create the heat with pressure of 0.75 bar for the acetylene. The tip of the torch was held ≈4.75 cm from the preform and moved up and down and around the preform to heat evenly and create a melt region of silicon at least 5 mm in length. Using a Minolta-Land Cyclops 53 pyrometer, the emissivity was set to ≈0.18 as that is the value of liquid silicon[54]. The temperature registered for a typical draw was around 1650 ° Celsius. From previous work done ([26]) it was clear that drawing rates changed the thickness of the fibre. It was therefore attempted to try and pull fibres consistently at the arbitrarily chosen rate: this was around 60 to 150 meters per minute.

3.3.5 Sample Preparation

For cross sectional analysis, the fibres were cut to a shorter length of around 1-2 cm. They were placed into a small metal tube that had been closed at one end. The tube was then filled with an epoxy resin and cured at 140 °C for 15 minutes. The tubes were then cut into 1.5 mm slices with a thin blade diamond saw. These were checked quickly to find the slice which presented the most and best looking fibre faces. This slice was then polished. As the saw cuts through the tubes with a grain size of around 200 μm they were initially ground with P120 (FEPA P grading), then P320, P500, P800, P1200, P4000. Final polishing to 1 μm was achieved by diamond spray in two stages of 3 and 1 cutting again. Each stage was considered to be complete when the face of the fibres presented were homogeneous in grind/polish marks. The epoxy is significantly softer than silicon and silica and so retained large gouge marks longer than the silicon. It was assumed these could also arise due to a "pile-up" of epoxy when being abraded, as they could appear at small grain sizes. This is noted as sometimes they could interfere with the fibre sample and this had to be recognised. As the fibres were clad in silica, which is an insulator, before they could be looked at in an SEM, they had to be coated with a conducting substance. One of the simpler materials to use as a coating is carbon. As carbon is a low atomic number (or commonly called 'Z') material, there are fewer electronic transitions that can take place and therefore less noise that is overlaid on the spectrum. As long as the coating is thin enough, the majority of the signal will still come from the rest of the interaction volume of the fibre below. It was attempted to carry out longitudinal cross sections of the fibres as well, with only limited success.

Chapter 4

Results and Discussion

4.1 Experimental process

As the process that was used was being used is fairly novel, it underwent quite a bit of development during its use. The following section discusses some of the the issues that were recognised and addressed.

4.1.1 Coating tests

It was noted that during the process of working with the tubes, the coating would become damaged and flake off from the sides of the tubes as the silicon was being loaded or in the process of drying. It was thought that this would, in the process of pulling fibres, cause issues as the silicon could come into contact with the silica, which has in other reports shown to be detrimental as reactions occur [14]. In order to remedy this, a few different possible solutions were attempted. This would hopefully increase the quality of the coating by improving robustness and homogeneity. Also there were complications that could arise from the coating method, such as using the hydroxide form to coat the preforms.

4.1.1.1 Pre-draw thermal decomposition

Previously in Chapter 2, it was reported that the thermal decomposition temperatures of the hydroxide forms of the oxides used are below the process temperature

used (see Table 2.3). It was also noted that the water groups, that would be created by this process have the possibility of bonding to the silica as hydroxyl groups which could then become a serious source of extrinsic attenuation in Table 2.1. To try to exclude this possibility, and also reduce the complexity of any reactions that could occur in the the tube further, it was therefore attempted to thermally decompose the hydroxide before loading the silicon and subsequent fibre drawing. This was carried out simply by placing the preform in a furnace and heating it to above the thermal decomposition temperature of the oxide coating and holding it at that temperature for 30 minutes. The furnace was then cooled slowly to minimise any thermal shock.

It was found that the coating became even more fragile when reduced to its monoxide form. Additionally, when using calcium oxide when performing the draw, if the tube was heated up to a higher temperature or for a slightly extended period it became more reactive with the silica, causing bubbles and holes to form. Therefore this method was disregarded for future draws.

4.1.1.2 Water content of the oxide mix

It was thought that a homogeneous and cohesive whole layer would perform better than a broken or uneven one. It was thought that by changing the viscosity of the slurry coating the lower viscosity would enable a more even coating of the slurry. This was tested by changing the water content for the standard calcium oxide mixture that was used as a reference throughout this thesis. The mixtures were then put onto slides to compare the differences between them. The more successful were also used to coat preforms to compare dried thicknesses. As can be seen in the comparison of the slide images 4.1, the change in water content did affect the coverage of the slide, Fig. 4.1a being among the best. It was discovered that it did influence both thickness and evenness. However while it is possible for the water content to be easily changed, it was not possible to control the thickness of the coating effectively by this method. This was due to the excess water forming runnels in the coating and draining through the coating rather than over. This is similar to those more apparent in 4.1b. When the coating had too little water in, a lower pressure had to be used to draw up the slurry, with too low a water content resulting in only a small amount of the oxide mixture being drawn in before reaching the limit of the equipment. Any slurry that was drawn in would be as likely to adhere to itself rather than the walls of the preform. This is probably due to silica's low root mean square of roughness [11] enabling the

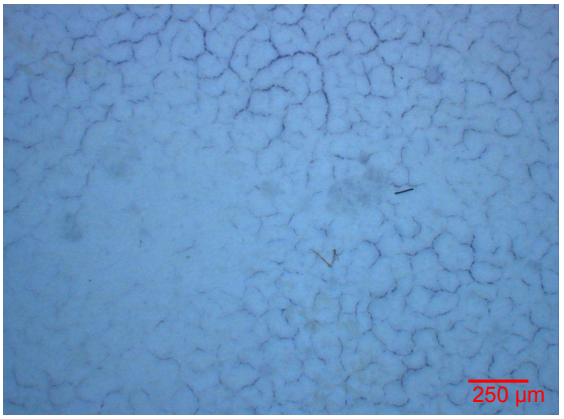

(A) Oxide with 3:1 water to oxide

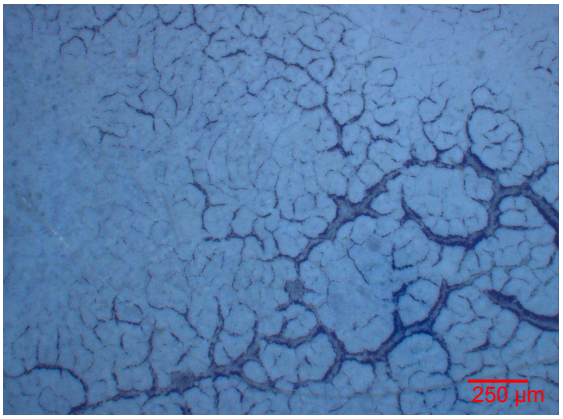

(B) Oxide with 3.02:1 water

FIGURE 4.1: Slides of coating performance with different water content

slurry slide off. The oxide which did remain was grouped together and led to a decrease of performance.

4.1.1.3 Coating draw rate

Associated with the trials with water content is the concept of drawing the oxide slurry of the same water content through the preform at a greater or lesser rate, controlling it with the vacuum used during the draw.

This was found to be slightly more successful than the changing water content, as with the optimal consistency of oxide slurry, a fairly even layer would form. This layer could become slightly thinner when drawn with more force. However, due to the denseness of the slurry as well as the lengths of the performs required, it was found that a relatively large mass of coating would be moved whilst attempting to produce a lot of fibre. As such a greater vacuum would be required in order to draw the slurry. This in turns was found to have knock-on effect; namely that it could lead to a rapid change in the velocity of the slurry.

4.1.1.4 Spin coating

A method to drain excess water and to smooth out the coating was considered, whereby the tubes that had been coated were spun. This could have allowed the

coating to settle into a more favourable position due to its higher density, letting the water flow off the top.

To carry this out, coated preforms were taken directly from being coated to a high speed stationary pillar drill. The tube was fixed into it and the tube was spun at 2400 RPM for 30 seconds.

This spinning method also suffered from causing runnels to form from the water separated from the coating. Another phenomenon that occurred was that clumps that would have preferably been smoothed were found to "snowball", travelling around the tube, gathering up more of the coating, rather than spread out. The result of this was similar to the runnels of liquid water, except small clumps formed after scraping small amounts of the coating away up to a small size.

In conclusion, spinning as a method of forming a better coating was also deemed ineffective.

4.1.1.5 Coating additives

In the processing of concrete, additives are often used to give the wet and hardened concrete different properties. As cement is composed mainly of calcium oxide, it was thought that by using similar additives, desirable properties could be obtained. The two that were decided on were a surfactant to act as a plasticiser to increase workability, and a bonding agent to help it stick to the silica tube. As a large effect can be obtained by the addition of a small quantity of additive, it was hoped that contamination would be kept to a minimum and restricted to the interface. Alconox named soap was used, as similar anionic surfactants are present in that which is also found in concrete equivalent [55]. The glue used was a water based polyvinyl acetate. A water based glue was used so it would have less difficulty blending with the slurry.

To test this hypothesis a small quantity of the slurry was made with the addition of a range of additive concentrations up to 10%. It was prepared using the slide method from the previous chapter.

The glue had the deleterious effect of causing the slurry to be more self-cohesive. Rather than sticking it to the preform, it preferentially clumped together more than previously. While it can be seen from Fig. 4.2a that it seems like a nice, even coating has been formed, this was actually due to the slurry clumping together

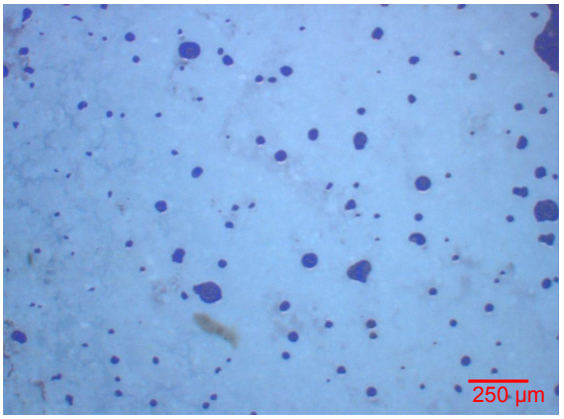

(A) 2% glue added

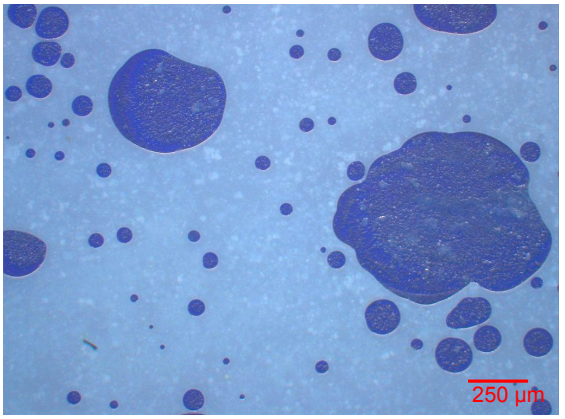

(B) 2% glue added with pressure

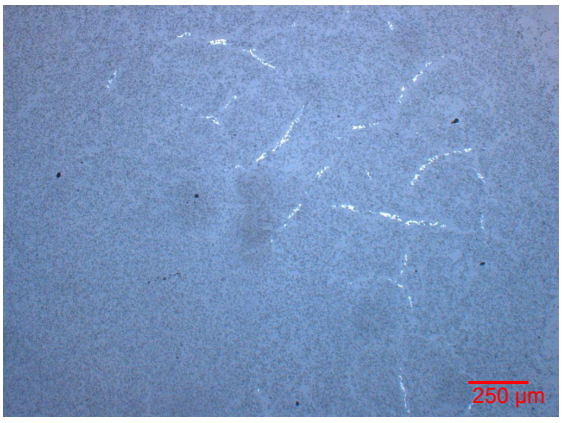

(C) 2% soap added

FIGURE 4.2: Slides showing performance of coating with additives

and becoming a lot more self-cohesive. This meant that the thickness of the drop was actually relative to the other samples formed, a lot higher. Subsequently, another slide was prepared where a little pressure was applied via another slide. This produced the effect in Fig. 4.2b. From this it was then attempted to create a balance by introducing more water that retained some of the cohesive properties that completed a layer, but was fluid enough for easy manipulation, however this never occurred before it returned to a high water content CaO slurry as in Fig. 4.1b. The glue also had the additional consequence of containing compounds and chemicals that were assumed would introduce complications into the process, and that the coating could not be definitively said to be better than a normal coating due to its workability, so this option was also abandoned.

Soap as a surfactant worked as expected, as less water was required to maintain

the same viscosity. The coatings formed appeared to be slightly more homogeneous and it was possible to draw lengths of continuous fibre up to 42 cm (see Appendix A.3).

4.1.1.6 Tetraethyl orthosilicate (TEOS)

The chemical compound is $Si(OC_2H_5)_4$ and in the presence of water it will react to form silica and ethanol [56]. It forms an interconnecting film of silica bonds. It was thought that by using TEOS as a finishing coat to the oxide, it would form a layer that was more robust due to the interconnecting bond. It would also provide a layer that covered any small defects in the coating that would arise from drying.

The TEOS was applied by taking a tube that had just been coated, however instead of drying completely, it was only placed in the drying cabinet for 15 minutes before being removed. It then had the TEOS solution passed through it a couple of times to ensure that all the coating was covered. This is because TEOS requires the presence of water for the reaction to produce silica, else it tends evaporate unreacted (when deposited at atmospheric pressure and room temperature) [57]. It was then returned to the drying cabinet overnight.

This presented the most promising method of sealing the coating and giving it a more uniform reaction to heating. However, it could be that problems arise due to it. The extra layer could traps more hydroxyl groups within it, allowing more to be retained in the interface region, which as mentioned in Chapter 2 absorbs greatly in the IR region. As these groups would be forced out upon heating, with a longer heating process this might not be such a problem. Unfortunately, using a burner and quick process such as this could result in some remaining to cause losses.

Using TEOS seemed to allow the creation of fibres that were more robust, which can be seen by what the fibres looked like after they had been etched in hydrofluoric acid when compared with other fibres Fig. 4.3. It seems that there are significantly fewer fragments of TEOS fibres present than for the others. While carrying out the drawing of fibres, TEOS seemed to improve the probability of success.

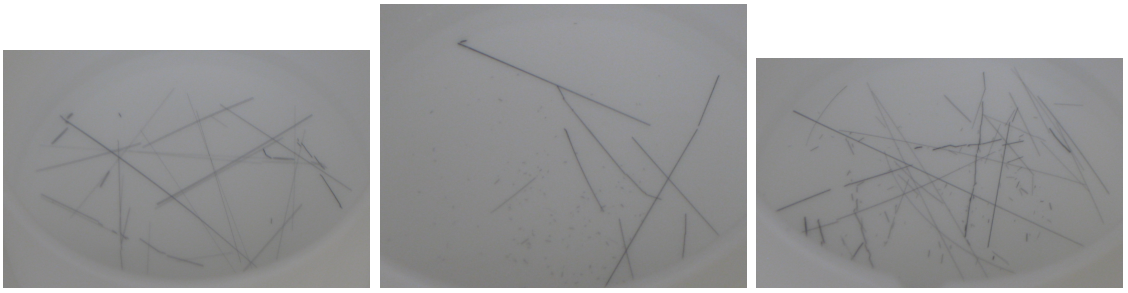

(A) Collection of TEOS etched fibres (B) CaO etched fibres (C) $CaO/MgOH_2$ etched fibres

FIGURE 4.3: Comparison of etched fibres

4.1.2 Fibre drawing

The two main parameters that are available to determine is temperature and speed. In changing these, it is possible to determine the size of the core [53]. In the case of this study, it is also interesting to see how the interface changes depending on the parameters used. With the level of control possible, it is difficult to determine precisely what is responsible for what aspects. This is especially true for the dynamic process of drawing, as there are more influences that modify the resulting fibre. For example, comparing Figures 4.4b and 4.4d, which came from the same experiment, a totally different interface is exhibited. The tube that was used was coated in the standard method, which makes it curious as to why there is such a large difference between them. In that case, the difference is likely to be the localised properties of the coating in that region and the movement of silicon as it melted as a powdered core was used, remembering that due to silicon shrinking on melting, it is very difficult to prevent any movement of silicon.

Similarly, Figs. 4.4a and 4.4c also originate from the same preform. In this case, the difference between samples is the core size and thereby the draw speed. However, one has an obvious and fairly large eutectic structure and the other appears to be without one.

In Figure 4.4d it is clear that, despite there being no obvious eutectic layer, there is a band of the modifier present. Not only does this modifier appear to occupy the outer layer of silicon, but there is evidence that there is a higher density of oxygen atoms on the cladding side of the interface. This is a very interesting piece of information and understanding in what form the oxygen is on that side

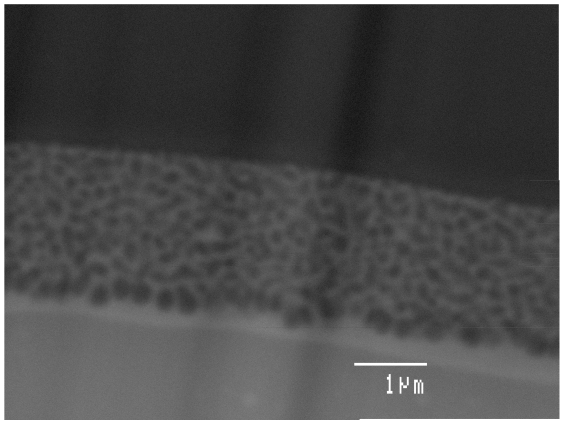

(A) Eutectic interface formed with SiO2-CaO-Si

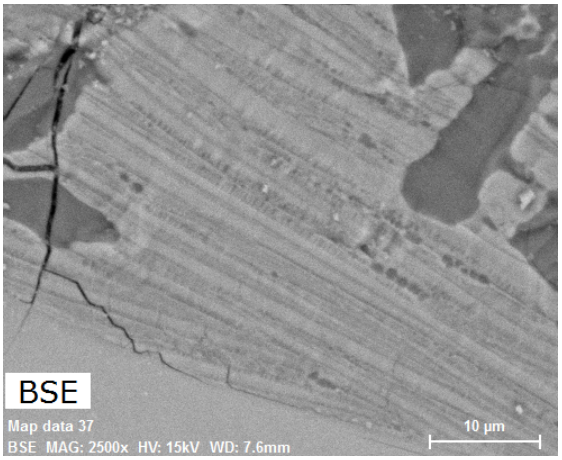

(B) Planar form of SiO2-CaO-Si formed from heating to 1550°C for 30 minutes, then cooling.

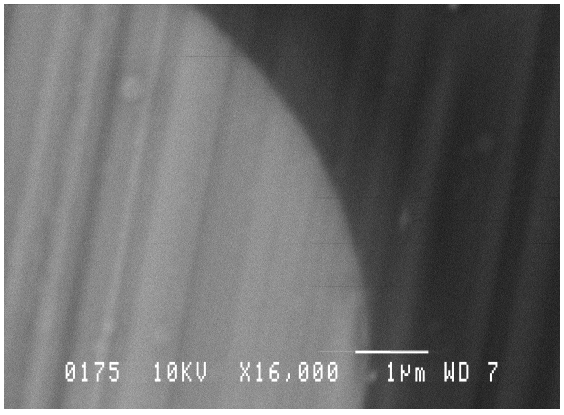

(C) Very thin interface with no visible eutectic

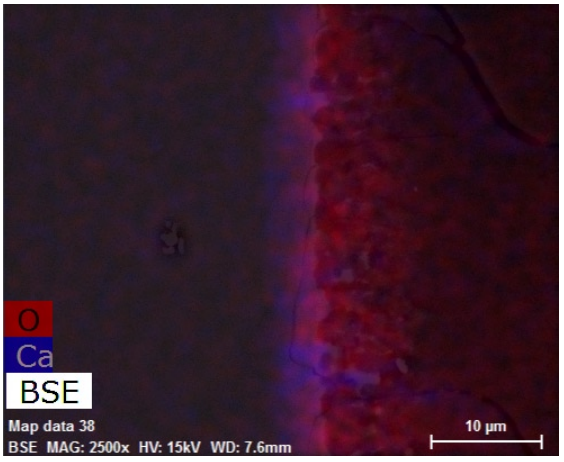

(D) Thin interface also from the slow heating as above but with rough interface

FIGURE 4.4: Variation in the interfacial layer.

is paramount to understanding which mechanisms yield the desired results out of those that are available to the system.

The eutectic structure that is visible originally in the Fig. 4.4b shows large plane like structure that is away from the interface, which is an indication of normal eutectic growth [38]. However, this changes completely when put into a dynamic situation such as when drawing a fibre, shown in Fig. 4.4a. At this point, the turbulent flow that is likely to arise at the interface between the highly fluid silicon [58], and the viscous silica/oxide combination causes a complex interplay between the cooling components at the boundary. The structure which is so formed, could be due to the mixing process, the taking up of silicon to form wollastonite, which would cause it to precipitate out. The transport properties of the compounds being used in this system are of interest, as this would determine the ease at which they can travel. Variations of this would be a factor in the final material composition if it is a more glassy or crystalline material. The parameters of such are system are complicated and can vary greatly with small changes of composition and pressure [59].

Looking closer at Fig. 4.4a it appears in the larger eutectic structure visible that the size of the silica groups are larger adjacent to the silicon core. The transport properties could explain this, as the pressure would vary depending on the size of the fibre being drawn. This could aid in determining why and what layer is between it and the silicon core. This could be a super-fine eutectic structure, another compound that is formed or just the oxide and silicon mixed from gradual cooling. As many of the thinner fibres created present with this type of interface, it might be that conditions were right to form an optimal interface layer for creating smaller fibres.

The thinner interface that is visible in Fig. 4.4d shows what seems to be an excess of calcium with not much or any oxygen inside the silicon core. This could be attributed to CaO being able to react with Si over 1000 K to form $CaSi_2$ [46]. This isn't certain as the details on how energetically more favourable to form this set of compounds is within the experimental error margin although in this case it appears to be supported.

4.1.3 Solid cores

Solid cores were made in response to the problems encountered in both loading silicon into the tubes and forming the melt region. When trying to form a melt

region within the preform situations can arise in which the local temperature became hotter than desired causing a reaction with the CaO coating. It was further noted that this did not seem to be happening or could be prevented by having silicon present. The silicon appeared to stabilise the region, which was assumed to be either due to its greater thermal conductivity conducting heat away from the local point thereby reducing the heat intensity; alternatively due to a boundary mixture being formed between the silicon and coating which prevented its reaction with silica.

4.2 Comparison of results

A critical factor in pulling a fibre is temperature. Temperature, while it may not be the only parameter that determines how quickly a fibre can be drawn, influences a lot of other factors such as the thickness of the fibre, reactions that can occur in the fibre and the rate of those reactions. The draw rate changes due to the increase in fluidity of the silica cladding as the viscosity of the silicon is so low. The oxy-acetylene flame reaches temperatures well over 3000°C [60] and hence could easily achieve the temperature required. It was attempted to vary the temperature by holding the flame at a distance from the preform. However, due to the method of heating by the intense naked flame, size of the sample, and silica interposed between them and the sensor, it was more of a rough estimate and guideline for future experiments.

Upon pulling a plain solid silicon core fibre clad in silica, in the vast majority of cases, the fibre that was pulled exploded. The thicknesses of the fibre were more difficult to get smaller and the fibres that were created tended to be a lot less flexible. This was attributed to the expansion of the silicon upon freezing. Despite this, it is possible to draw whole unbroken sections of solid cored fibre in this manner.

In Ballato's paper [13], it was stated that they chose to create a thicker walled tube to "[...] mitigate potential issue with the weight of the molten silicon leaking out or otherwise deforming the softened cladding glass during the draw." It was found that this occurred to some extent when the preform was heated enough, the molten silicon dissolved the silica cladding. However, this was not the dominant form of deformation. During the extending heating trials when the heating was applied for any length of time in one direction the combination of heat and gas

flow from the burner tip blew the preform away. Consequently, in the method described earlier in Chapter 3 reactions between silicon and silica which caused oxygen leaching into the core did not occur as it was performed quickly. This is evidenced by Figure 4.7b which shows the short transition from cladding to core levels. There may be a slight step; however, as it is at the limit of detection on the EDS it is uncertain.

In Ref. [61] they use a method of stacking smaller preforms within a larger. When this preform is then drawn, with uniform heating it effectively scales down the preform to the same relative dimension. An attempt was made to replicate this by using a "fibre in fibre" method in an effort to produce smaller fibres. This was carried out by preparing some premade fibres and placing them into another tube preform. This would hopefully have the result of creating even smaller fibres within another fibre, hopefully bringing the size of the fibre into single-mode region. However, due to the size of the fibres already being fairly small (10 - 50 μm) and it being very time consuming to make vast quantities of fibre, it was required to pad the tube. This was done with a little silicon and coating the inside of the larger preform and outside of the fibres. While there was little concrete evidence of succeeding in what was hoped, it was still possible to draw fibres. In retrospect, it may have been more productive to obtain smaller tubes or capillaries to fix the fibres into position and to fuse them together before attempting a draw.

Raman spectroscopy was also carried out on fibres that were made in this method [62], it showed that there was a high degree of crystallinity which is similar to that which was seen by Ballato [13]. This should mean that over the distance that the fibre is present, it would react like a crystalline sample of silicon. However optical losses of the fibres was found to range between $\approx$2 and 50 db cm^{-1} with the modal being around 4.2 db cm^{-1} [63], which is comparable to that currently obtained through the molten-core and powder-in-tube methods [13, 26, 64]. However, there is more variation in fibres of the same construction. It is believed that the losses that arise are due to the more artisanal nature of the process and superior fibres could be created by introducing more of the techniques used by Scott et. al. in their work.

On many of the samples that were produced and looked at, there was a slight raise or "ledge", indicating an increase of oxygen concentration. This ledge is prominent in Figures 4.8b, 4.8c and 4.9b, and was originally thought to be on the side of the heating and came about due to possible oxidation of the silicon from damage from ablation due to the flame. From looking at Figure 4.5b it looks like this could be

the case. The data is a little misleading though, as the flame is so concentrated, once it heats the silica up to a certain point the thrust from the torch pushes the preform away. As the preform is then not only further away, but at an angle to the tightly focussed flame, it experiences a lot less temperature. It is possible there are variations along the preform that would cause heat to transfer anisotropically through the melt region.

This could also be a result due to formation of cristobalite, or some other unwanted phase from water and hydroxyl groups being driven from the hot side but forming or remaining on the other, crystallising into possibly unwanted phases. This is unlikely though, as the EPMA results don't show a high enough density of oxygen for the other phase of silica.

It seems likely that the step is present around the entire circumference of the fibre. As it is likely a result of the directional heating it will be more prominent at the edge that faces towards the heat source for the longest period. This could arise as the torch ablates the surface of the silica cladding in the process of creating a hotter local region on the preform which leads to a faster rate of reaction between the silica, coating and silicon system. This is supported somewhat by taking Fig. 4.5a into consideration as well, and noticing there is a lack of any prominent step for any of them relative to any of the others. Assuming that this slight step exists in all fibres either none of them have a slight step or the resolution of the SEM EDS could not get good enough resolution. Although by also looking at the different angles in Fig. 4.5a it is possible that there is indeed an increase in the oxygen concentration before the rapid increase in oxygen.

From the data collected from the EPMA i.e. (e.g. Figure 4.9b, 4.8b and 4.8c) it becomes noticeable that the step that occurs is approximately the of the same height as that of the coating that is used. This suggests that oxygen is being dissociated from the oxide coating into the silicon. Looking at the phase diagram of the CaO systems 2.5, this shows that at the operating temperature it is likely there will be a liquid slag composed of silica, calcium and elemental silicon. As the temperature cools there will be a solidification of the coating and silica; however, at this temperature by using [44] it calculates that there is still the possibility of a eutectic mixture between CaO and elemental Si existing. Consequently, this leads to a complex situation which is not totally understood as there is a lack of thermodynamic data [46]. One can only suspect that in the interplay between the compounds leads to the same amount of oxygen from the original CaO being dissociated or being absorbed by the silicon. Although it is interesting with this

result that it runs counter to that stated about Fig. 4.4d, as instead of forming a calcium silicate ($CaSi_2$) oxygen has instead leached into the core. It is possible that it does form, as noted in the stable situation of 4.4d, but then due to the flow and turbulence, is mixed with the CaO and SiO_2 eutectic slag, which then is likely to react with the silica [44, 46]. However, this does not seem to cover all aspects as in the EPMA results it shows a fairly clear separation between the coating material and the silicon core and whatever oxygen is present. Whilst this could be just due to the nature of the reaction, that it leaves a level of coating below detection limits, it seems improbable. To make any definitive conclusion would require more detailed examination of the interface and the interactions taking place.

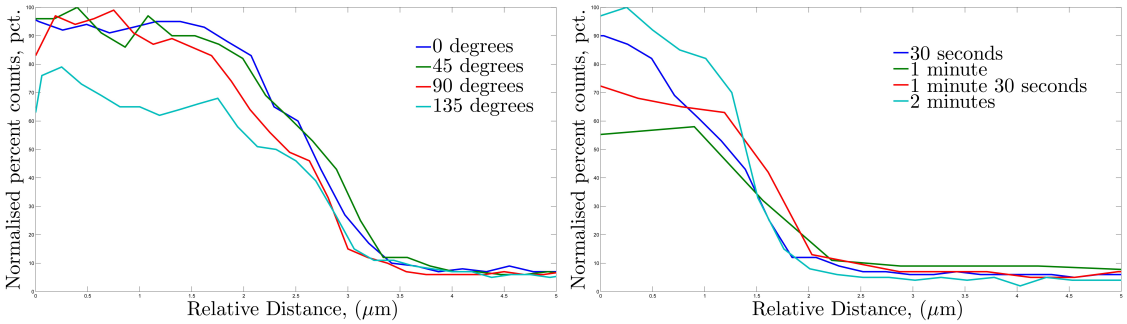

(A) Showing different cross sections from the same fibre

(B) The same fibre with different times heating before drawing fibre

FIGURE 4.5: Looking at how the oxygen concentration varies to heating direction and time

Bending fibres is problematic, as they would suddenly break very quickly and it could be difficult recording the correct values. Also, it is a destructive method, sometimes shattering the fibre along a significant length into small bits. Regardless of this. the flexibility of fibres has been rather good, achieving bending radii down to as low as 0.5 cm. The more common is shown in Fig. 4.6 and larger ones in the Appendix A.2.

This is an indication of a fibre that does not have many defects in its core, as from Figure 2.8, the existence of larger and many flaws increases the chance of a fracture and break at lower stress from even large bends.

Using EDS, it is impossible to study strontium as the strong Kα x-rays are a little too high energy for the Hitatchi TM3000. due to only its L-shell characteristic X-rays being very similar to those of silicon's Kα, and as silicon is present in a greater quantity it overshadows the signal, giving it greater weight. This can be

FIGURE 4.6: Bending radius of a $CaO/Mg(OH)_2$ fibre.

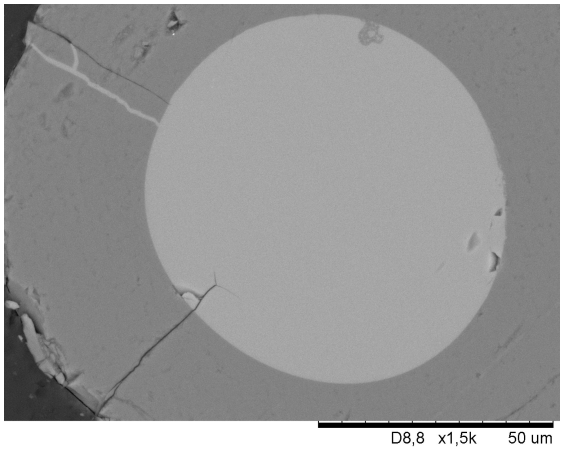

(A) A typical cross section view of a fibre without a modified interface

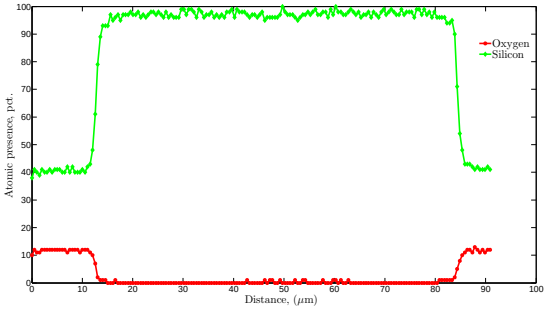

(B) EDS cross section through Figure 4.7a

FIGURE 4.7: Silicon fibre without modifier

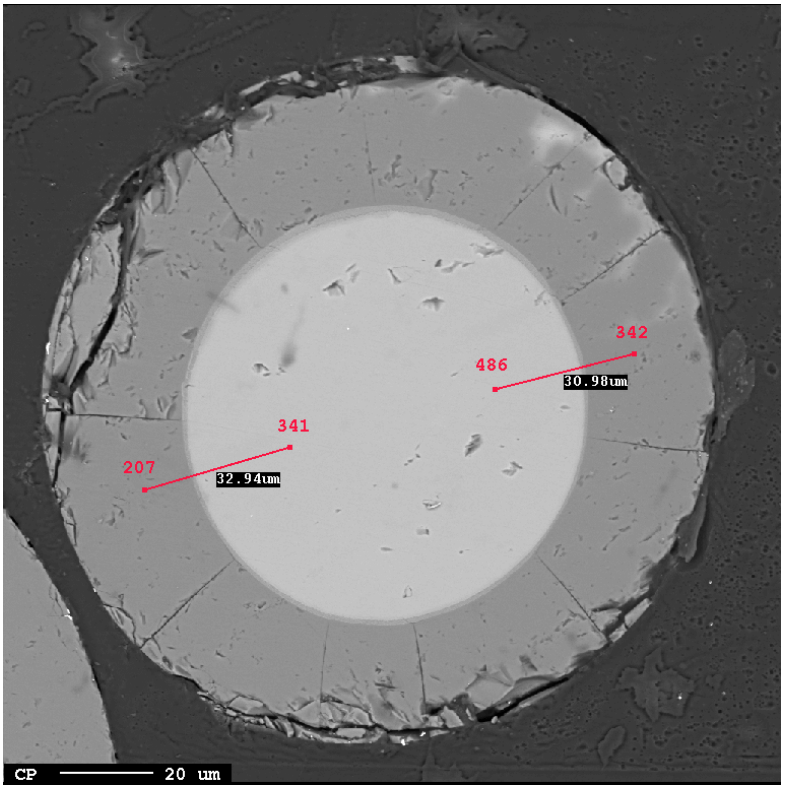

(A) Microprobe image and approximation of sampling path

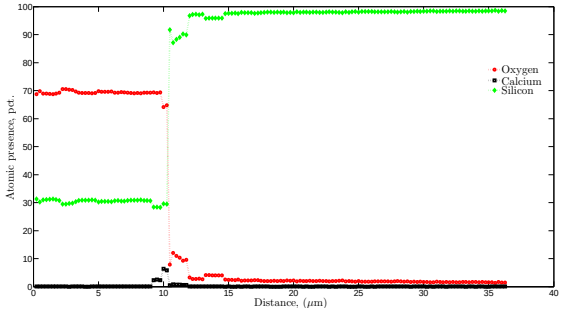

(B) Left side path

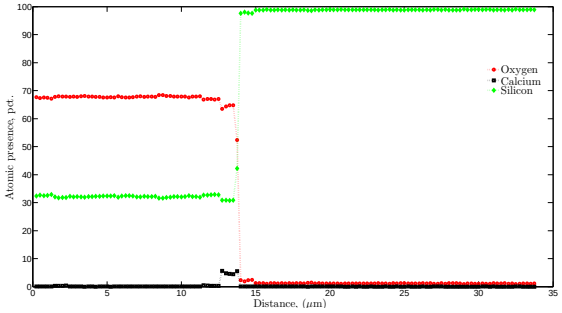

(C) Right side path

FIGURE 4.8: CaO interface fibre

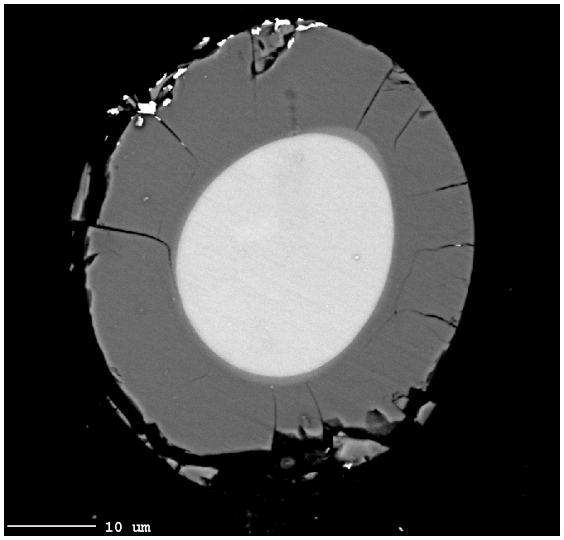

(A) Cross sectional image of fibre from which results were obtained

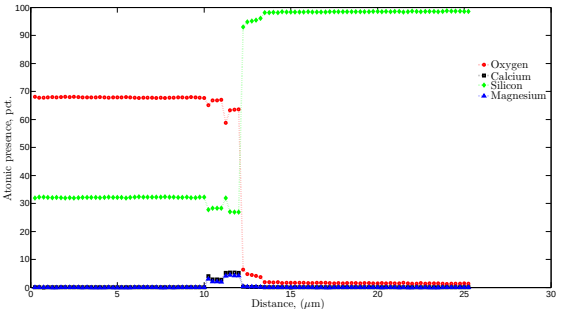

(B) Microprobe results from fibre

FIGURE 4.9: Microprobe results for a fibre with a $CaO/Mg(OH)_2$ mix interface

shown by the x-ray spectra collected in Figure 4.10. This spectra (4.10) shows the

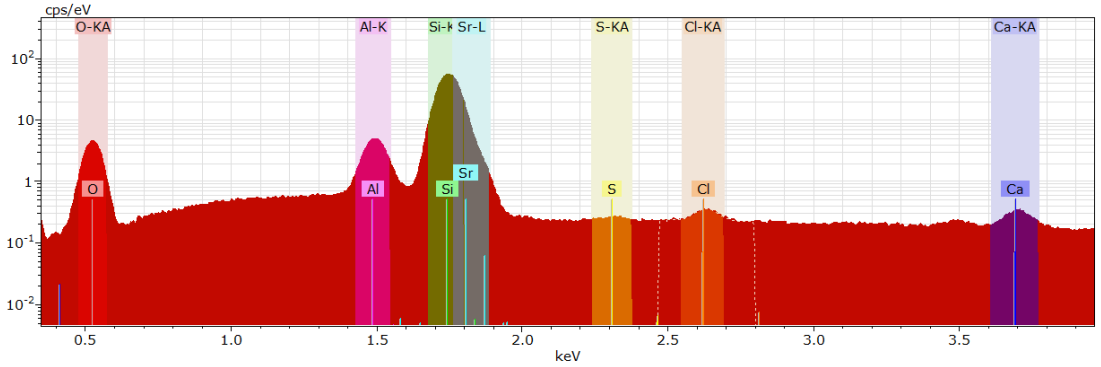

FIGURE 4.10: Spectra from strontium/calcium fibre sample

number of peaks per kilo electron volt (keV), which translates to the electronic energy levels that the electrons transition between. All of the peaks that are visible in the spectra have been identified and labelled apart from one. That one is just to the left of the furthest right calcium. This peak is actually another silicon peak. It is a phenomenon that comes about due to the measuring mechanism and the sheer number of silicon x-rays being created. The x-ray sensor has a finite response time, so it effectively takes the integral of energy for a certain period of time. If two x-rays hit the sensor in this time, they will be measured as one. This can be

avoided with the use of a discriminator, that discards measurements that are too close together. However if there are a lot of them, and they arrive often enough, they can cause a pile-up effect. In this case with one very large signal from silicon it is a signal that is at double silicon's peak. As silicon's kα is at 1.7 keV this pile-up peak is at 3.4 keV which it appears to be. The chlorine and sulphur that are present are most likely due to the epoxy that was used to mount the sample in, and the aluminium from the SEM mount and all the supports and facing inside the tabletop microscope. It is obvious from this spectra that the signal between silicon and strontium would get confused. From the strontium oxide results despite the

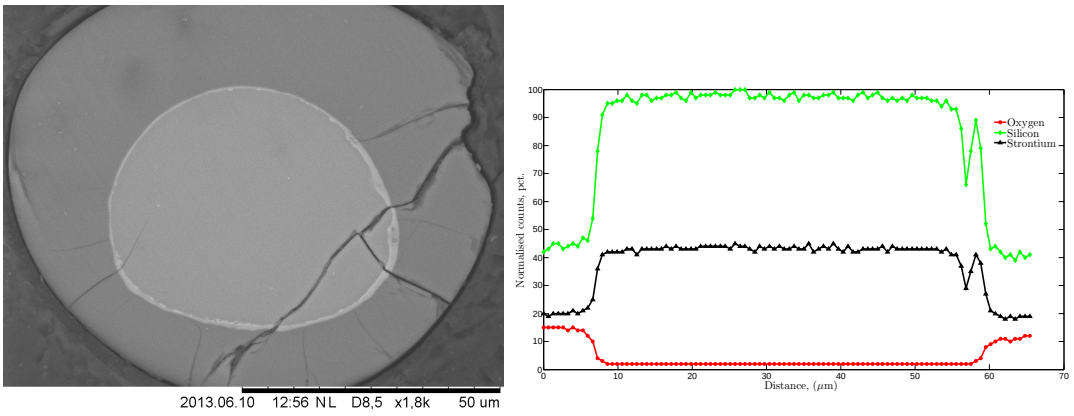

(A) BSE image of cross section of strontium fibre

(B) EDS cross section

FIGURE 4.11: Strontium compound interface

strontium showing a strong presence in the core, the oxygen and silicon behave as would be expected and has been seen in both the silicon only and CaO fibre. However it should be noted that drawing the SrO fibres was significantly more successful than silicon with no interface modifier, as the fibres did not explode on rapid cooling. The strontium and calcium blend however was less successful. It was difficult to pull a fibre with a continuous silicon core. Those that were pulled were fairly short around 5 cm long. The line scan from the EDS in 4.12b shows a noisier signal compared to 4.11b which could be an indicator that there is a reaction between the strontium and calcium oxides which may involve silicon. Either way it seems to also show a greater movement of oxygen into the silicon core. After returning to strontium despite the poor results from the initial testing, the fibres that were created seemed to be better than expected. It could be that as the carbonate form is being used and in the primary study the conditions were static and almost horizontal. The maximum temperature was also a lot lower, so the inclusion of the carbonate caused the compounds and precipitates formed via

it thermally decomposing caused problems later on, however when being used in fibres, not only was a higher temperature used, but a more complex system in general was present with the dynamic motion of silicon through the draw region. $SrSiO_3$ is lattice matched with silicon so it might be a good to investigate as it could provide a basis for a more monocrystalline structure. Although from the samples that have been made with strontium, it could be fractures with strontium compounds involved are more likely to penetrate into the core, or cause larger fractures inside visible in Fig. 4.12a which was fairly typical.

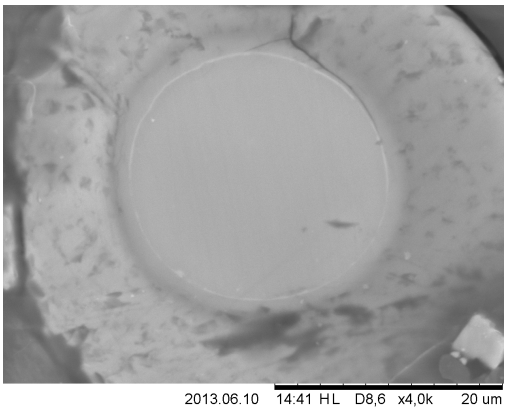

(A) BSE image of cross section of strontium and calcium fibre

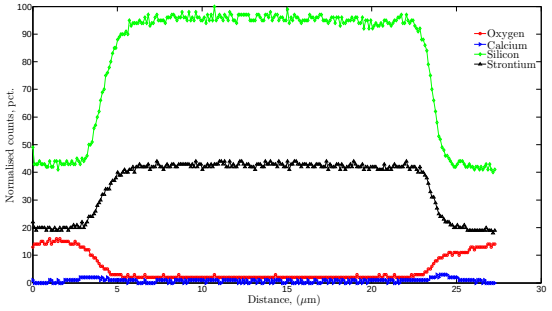

(B) EDS cross section.

FIGURE 4.12: Strontium carbonate and calcium oxide interface

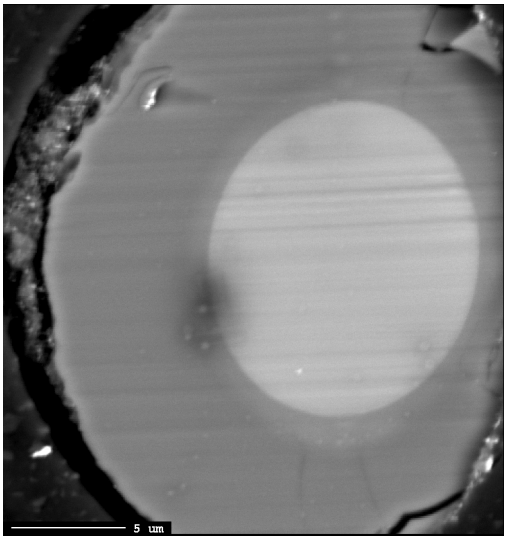

(A) Fibre in fibre CaO coating only

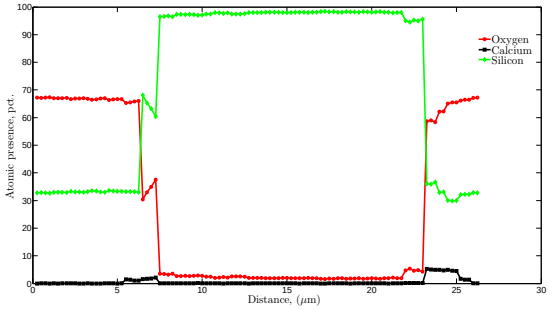

(B) EPMA results from 4.13a

FIGURE 4.13: Fibre in Fibre with calcium oxide interfaces

The fractures that have formed in the fibres above haven't always formed in the silicon when it expands, but rather in the silica and it has propagated towards the core. Although it is uncertain whether this has taken place due to the polishing, or another process is contributing to it.

The SIMS results show the different counts of impurities within the silicon bulk that is being tested. The graphs show that the impurity difference between the polysilicon 4.14a and 4.14b used to create the silicon cores and the NORSUN wafers 4.14c and 4.14d are not that different. The NORSUN wafer has less more massive impurities than the polysilicon reaching the limits of accuracy of the SIMS. It shows that the NORSUN wafer has greater concentration of impurities on the surface. but that it drops slightly below that of the polysilicon. Looking back to Table 2.1 it shows that the only real impurity that is present in both of them is carbon. From comparing these sources of silicon to the 4.14f and 4.14e it shows that there is very little increase in the impurities. All the concentrations apart from calcium and titanium and boron have remained at about the same level as the source wafer. Calcium was used in the fabrication of the fibre so it is not unusual that it should have increased, however it is somewhat surprising that it has not increased more than what is recorded. The assumption here is that is the heating and subsequent freezing was rapid enough to not give enough time for diffusion that far into the material. However, as the concentration is relatively constant with depth it may be that it did not diffuse more as the calcium is tied up in larger compounds that are not as free to diffuse for some reason. The low impurity count reduces the Rayleigh and Mie scattering events and extrinsic absorption.

The fibre that was used here in Figs.4.14e and 4.14e was using the high purity n-type NORSUN wafers. However, there appears to be contamination from a boron source or a confusion of samples, as it shares more in common with the polysilicon sample. As can be seen from the SIMS plots. It would possible be worthwhile performing a SIMS analysis on a fibre that was created from the polysilicon to see if increases the impurity was indeed due to a mix up or there is a point in the method where contamination occurs.

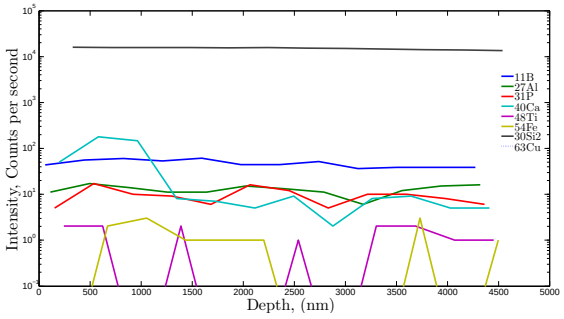

(A) A poly silicon sample using oxygen primary ions

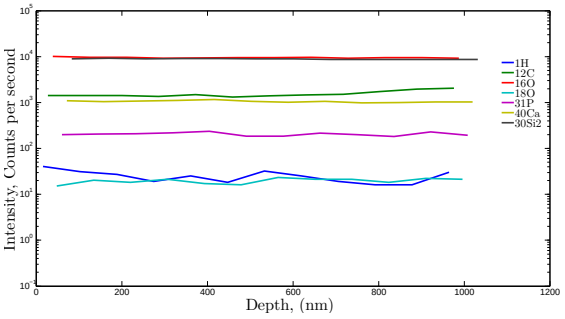

(B) A poly silicon sample using caesium primary ions

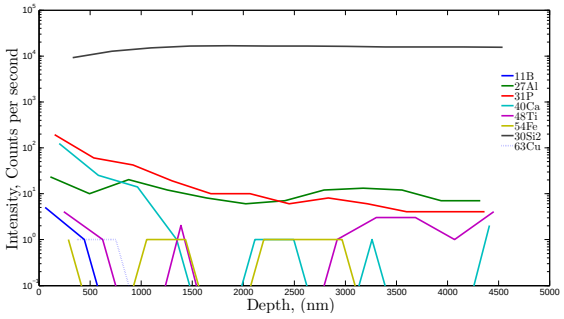

(C) A NORSUN wafer using oxygen primary ions

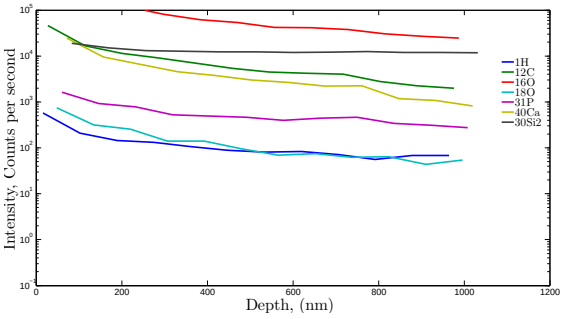

(D) A NORSUN wafer using caesium primary ions

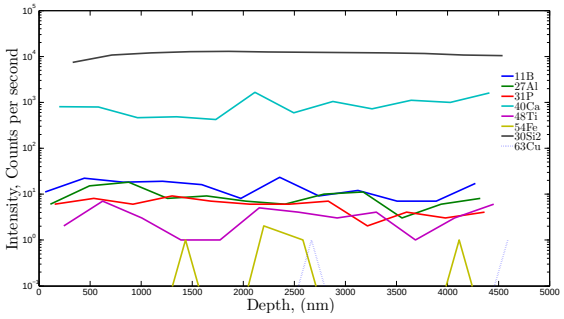

(E) A NORSUN fibre using oxygen primary ions

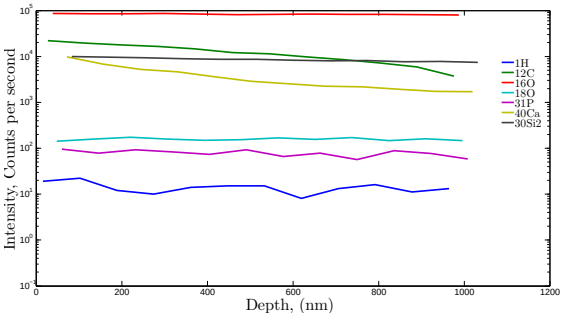

(F) A NORSUN fibre using caesium primary ions

FIGURE 4.14: SIMS results using raw data only for comparison

4.3 Interpretation

Cristobalite growth could be exacerbating any damage that occurs. As often there is significantly more damage at the surface of the silicon core, and this is where cristobalite growth can be found to originate. This could occur due to the hydroxide nature of the coating that is put on, with the fibre being pulled quickly after being heated. Bubbles could be seen when heating the preform, even when it is well below the boiling temperature of all materials. This is most likely steam from the decomposing hydroxides.

Elemental silicon is unable reduce magnesium oxide, or any magnesium silicate compound which makes it a rather inert substance to use, indicated by the stable tie line in Fig. 2.6a and the higher eutectic point in Fig. 2.6b. This could explain why it was so difficult to pull and create any appreciable sample when using a pure magnesium oxide coating. Silicon can reduce CaO [47]. It has been noticed that there often is a noticeable second interface layer aside from the more obvious eutectic. This layer forms between the eutectic and silicon when using CaO. As mentioned earlier, MgO is stable with silicon and once CaO has reacted with silicon to form a stable silicide, it would remain inert. This could be forming a layer that then prevents any further reaction and hence stopping the transmission of more impurities into the core.

As discussed previously, calcium oxide and silicon react to form $CaSi_2$ and Ca_3SiO_5 at 1000 K (≈727°C) which is higher than the thermal decomposition temperature of $CaOH_2$, so it is entirely possible this is formed while the bulk silicon is still solid. This could explain the small amount of infiltration of Ca from SIMS results, but as it wouldn't react that much as the reaction is not that favourable it might not allow so much [46]. Wollastonite has a thermal conductivity of around 2.7 W m $^{-1}$ K $^{-1}$ It also has a high thermal shock resistance. Density of wollastonite measured = 2.86 to 3.09 g cm^{-3}, its calculated density is = 2.90 g cm^{-3} [65]. It is likely that the uneven surface from an irregular draw rate, and therefore core/cladding interface can disrupt the growth of the crystal structure, reducing the size of the grains as the orientation of the surface would have preferred orientations of crystal.

Determining the optimum thickness for the coating layer is going to be a challenge as it the mechanism of how the interface contributes to improved fibre performance. If by studying some of the EPMA results, it can be seen that oxygen does cause this small step inside the core. While it could be argued that the oxygen is being supplied by the oxide, by looking at the phase diagrams for calcium, it can be seen

that wollastonite would be formed as a stable compound. This would, for every atom of oxygen introduced due to the coating, be taking up two extra.

There is a definite advantage in the combination of the inert magnesium oxide and the reaction of calcium oxide with silicon/silica. This was seen from the size and flexibility of the fibres that were created. It provides a good combination to stop any reactions between the two. The wollastonite takes up silicon into a denser structure and has good thermal shock properties [65]. It is stable and hence does not react with the silicon any further. It is possible that the dense layer provides a little support for the silica containing the expansion of silicon to some extend. There seems to be a little more calcium in the core of the strontium mix one, but as only an EDS analysis was carried out, it's hard to say for sure. The thermodynamics between wollastonite and silica needs to be looked into in more detail. By using FactSage program, it can be calculated that wollastonite and silica have a eutectic point that is around the same temperature that of calcium oxide and silicon. This could indicate a more complicated relationship at the interface than was originally envisioned. When the system is heated to a point where silicon and calcium oxide are forming a eutectic, wollastonite could precipitate out of the Si/CaO mixture. Then it could be mixed via the turbulent flow that is likely occur during the draw forming an interplay of layers. If this is the case, it would require the re-examination of certain assumptions that are made.

4.4 Improving quality of fibres

There are multiple directions that could be taken which would result in an improvement of manufactured fibre. Work has already progressed into developing a system that would be a lot more controllable: multipoint fixed distance heating, fixed draw speed. Once there is a system for better controlling the fibres growth, as in Scott's work, there is a great opportunity to further define the mechanisms by which these interfacial layers work.

Fibres were able to be pulled using the conventional fibre tower at Clemson with the aid of Ballato's colleagues. These were pulled using a preform created by the author in the same method described in Chapter 3. The fibres that were drawn there had a surface roughness that was superior to those drawn here which is evident in Fig. 4.15.

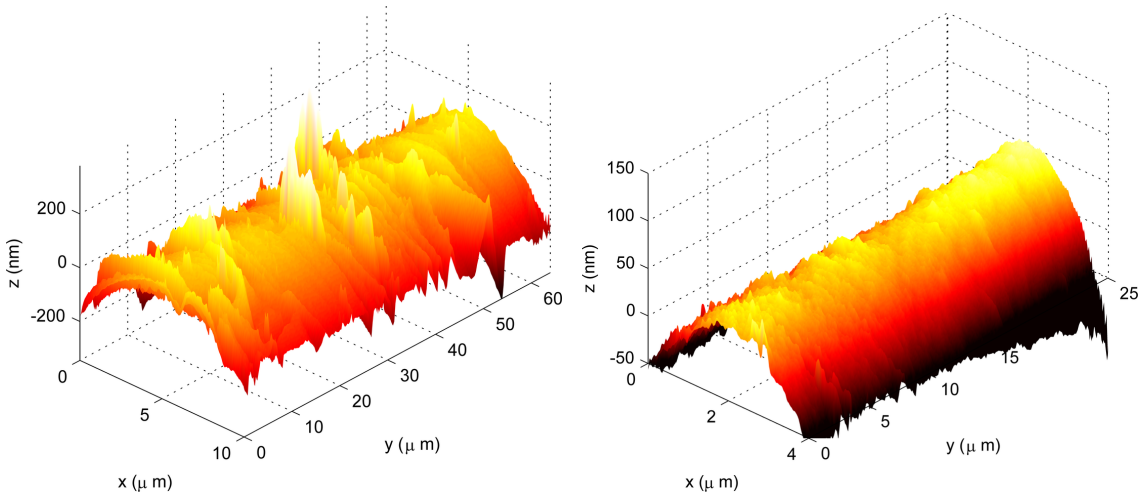

(A) Drawn manually. (B) Drawn at Clemson.

FIGURE 4.15: Comparison of surface quality from same preparation of preform, drawn manually and at Clemson.

Asymmetry in optical fibres is another factor that can introduce losses. Despite it being possible to make circular fibres, when looking at the fibre image cross sections, there are frequent asymmetric and symmetric variations in diameter. It is assumed that these variations occur due to the directional heating and manual nature of the draw in the main part although it could be exacerbated by the quality of the coating. It was discussed in Scott's work in Ref. [53] that grains grow into the centre of the fibre, the growth velocity of grains is different for different orientations. Over the thickness of 40 nm however, it becomes driven by kinetics of the system [66]. This suggests that the layer immediately adjacent to the coating of silica will be influenced. It is possible that with post processing of the fibres a greater degree of crystallinity will be observed. However, there are total fractures that cause the fibre to fall apart on etching; hence, it would probably require fully re-melting the silicon core, which might lead to diffusion of impurities. The presence of full, cross-core, fractures will probably be reduced with improved system for drawing.

4.5 Future direction

To carry forward to the research in this field, a system of controlling the drawing of fibres is of utmost importance. This requires being able to control the temperature

more effectively and controlling the drawing speed. Secondly it is important to improve on the coating process. While good quality coatings can be obtained via the in place process, making them more reliable and quantifiable will aid in future investigations and be able to conclude whether it is necessary to have the coatings that good. Being able to explore at a closer level if there is a eutectic structure that is just too fine for the SEM to pick out will go far to determining if it is indeed due to a eutectic that the stress of expanding silicon is absorbed.

The chemistry of the interface while initially appearing relatively simple leads to a series of interconnected processes, understanding how these affect one another will provide insight into the mechanism of creating an improved fibre. This could suggest an optimum modifying oxide to silicon ratio that would decrease the surface oxygen content of the core.

A result of some of the theories discussed in the above chapter is that the tension generated from expanding silicon. To determine whether this stress is absorbed in the silica cladding or the oxide layer, a study into the claddings birefringence could reveal how much stress it is under. This could go some way to determining the mechanism which allows longer unbroken fibres to be formed.

Chapter 5

Conclusion

It has been shown that greater mechanical stability can be produced in solid silicon core optical fibres using an interface modifier. A very low impurity content has been shown to exist using EPMA and SIMS analysis on produced fibres. The optical losses of fibres manufactured have been of comparable magnitude.

It has been shown that a eutectic can form at the interface, and that fibres drawn using an interface modifier to exhibit increased robustness. However, it is not entirely clear whether this is due to the initial hypothesis of the eutectic layer. It could be due to the prevention of the detrimental reactions between silica and a silicon. This would decrease the amount of damage sustained by the silica and therefore when the silicon expands it does not have a weakness to exploit that causes the fracture.

Post etch, the fibres often fragmented, indicating that there must be fractures within the core of the fibre. These fractures would probably be a large portion of the observed losses in the fibre.

Roughness of fibres does impact on the transmission properties of the silicon. Microfractures are likely to be a problem, which the author believes would be partially solved by a more even heating system and a more thorough deposition method of the coating. It would be beneficial to investigate the thickness of the interfacial layer.

Appendix A

Additional images

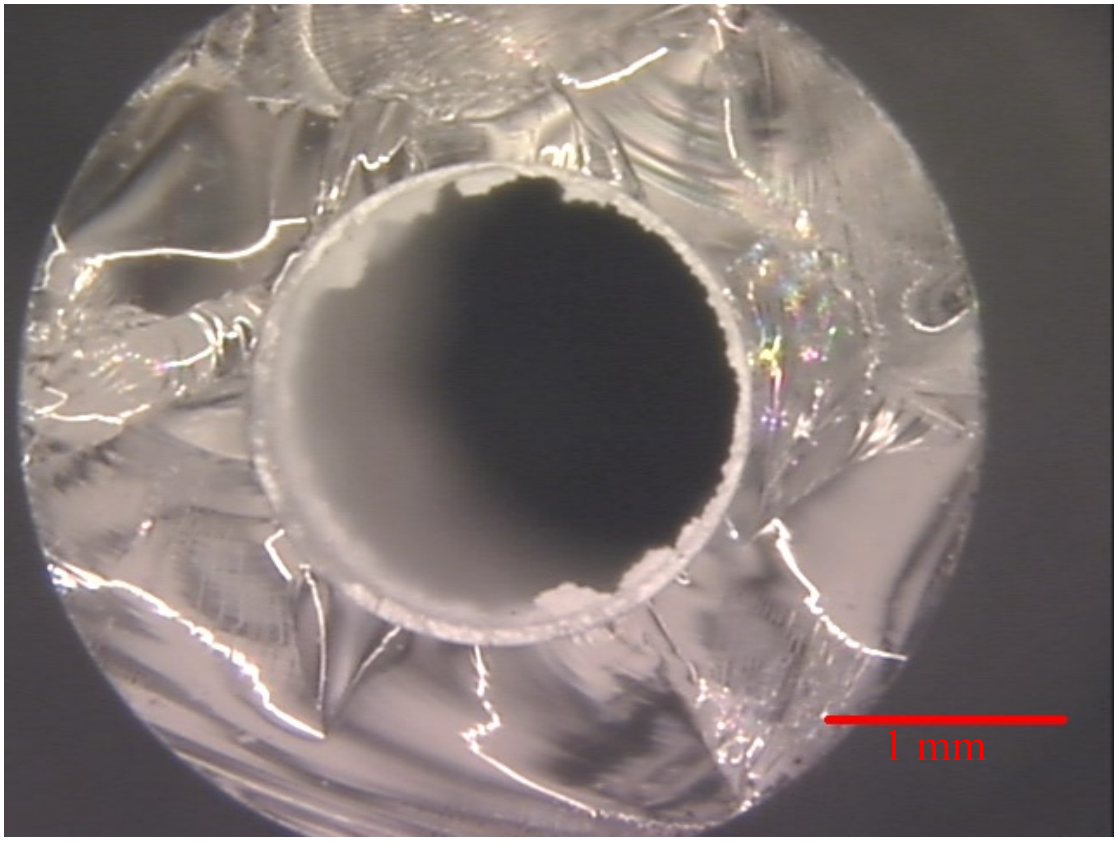

FIGURE A.1: Calculating the coating thickness of the preform by direct measurement.

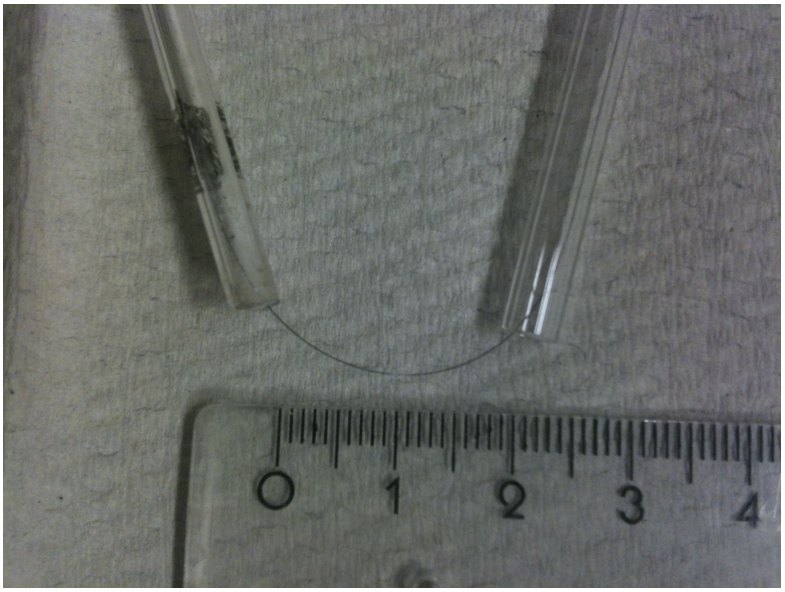

FIGURE A.2: Another fibre being bent to find bending radius.

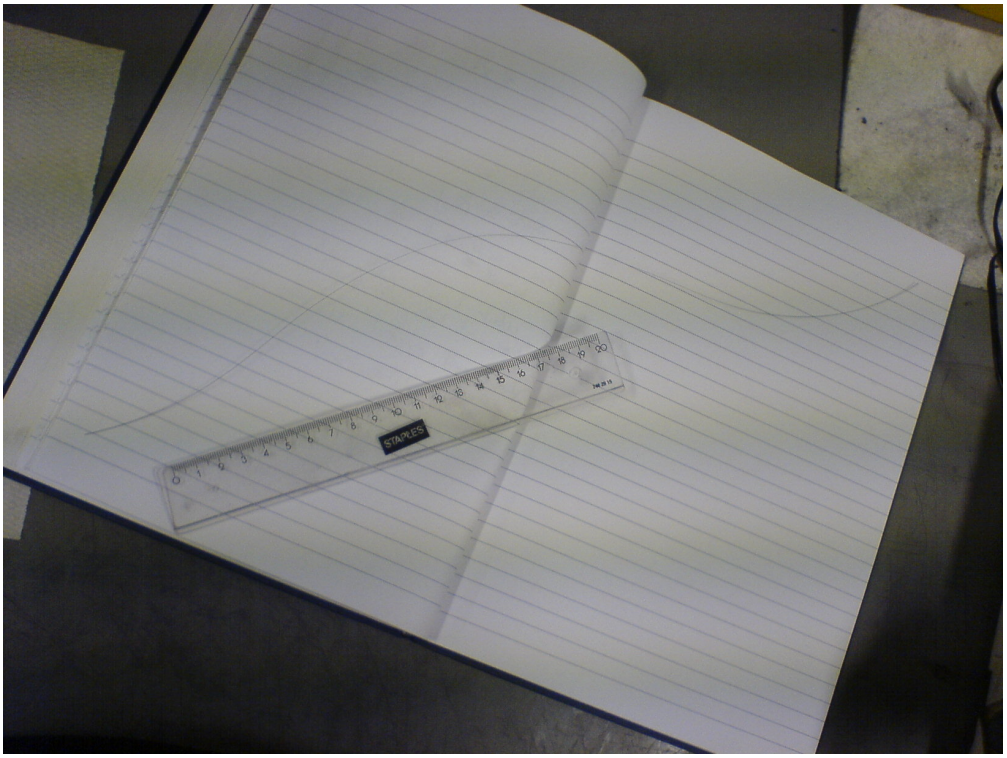

FIGURE A.3: A long stretch of fibre.

Appendix B

Important additional paper

Alkaline oxide interface modifiers for silicon fiber production

Erlend F. Nordstrand,[1] Andrew N. Dibbs,[2] Andreas J. Eraker,[2] and Ursula J. Gibson[2,*]

[1]*Department of Materials Sciences, Norwegian University of Science and Technology, 7491 Trondheim, Norway*
[2]*Department of Physics, Norwegian University of Science and Technology, 7491 Trondheim, Norway*
**ursula.gibson@ntnu.no*

Abstract: We demonstrate the ability to pull small diameter silicon-core fibers with low oxygen content by using interface modifiers between the silica cladding and the semiconductor. Alkali earths scavenge oxygen and form a fine-structured eutectic that accommodates thermal strain and may be useful as an intermediate index cladding layer for optical applications. NaO, MgO, SrO, CaO and BaO interface modifiers were tested. CaO coated fibers were made with core diameters down to 10 microns, small bending radii, low oxygen incorporation, and optical losses below 4 dB/cm at 1.55 microns.

OCIS codes: (060.2280) Fiber design and fabrication; (060.2290) Fiber materials.

References and links

1. J. Bei, T. M. Monro, A. Hemming, and H. Ebendorff-Heidepriem, "Fabrication of extruded fluoroindate optical fibers," Opt. Mater. Express **3**(3), 318–328 (2013).
2. M. Saad, "Indium fluoride glass fibers," Proc. SPIE **8275**, 82750D, 82750D–6 (2012).
3. A. Peacock and N. Healy, "Parabolic pulse generation in tapered silicon fibers," Opt. Lett. **35**(11), 1780–1782 (2010).
4. D.-J. Won, M. O. Ramirez, H. Kang, V. Gopalan, N. F. Baril, J. Calkins, J. V. Badding, and P. J. A. Sazio, "All-optical modulation of laser light in amorphous silicon-filled microstructured optical fibers," Appl. Phys. Lett. **91**(16), 161112 (2007).
5. L. Lagonigro, N. Healy, J. R. Sparks, N. F. Baril, P. J. A. Sazio, J. V. Badding, and A. C. Peacock, "Low loss silicon fibers for photonics applications," Appl. Phys. Lett. **96**(4), 041105 (2010).
6. B. Scott, K. Wang, V. Caluori, and G. Pickrell, "Fabrication of silicon optical fiber," Opt. Eng. **48**(10), 100501 (2009).
7. J. Ballato, T. Hawkins, P. Foy, R. Stolen, B. Kokuoz, M. Ellison, C. McMillen, J. Reppert, A. M. Rao, M. Daw, S. R. Sharma, R. Shori, O. Stafsudd, R. R. Rice, and D. R. Powers, "Silicon optical fiber," Opt. Express **16**(23), 18675–18683 (2008).
8. J. Ballato, T. Hawkins, P. Foy, B. Yazgan-Kokuoz, R. Stolen, C. McMillen, N. K. Hon, B. Jalali, and R. Rice, "Glass-clad single-crystal germanium optical fiber," Opt. Express **17**(10), 8029–8035 (2009).
9. B. L. Scott, K. Wang, and G. Pickrell, "Fabrication of n-type silicon optical fibers," IEEE Photon. Technol. Lett. **21**(24), 1798–1800 (2009).
10. T. Minami, S. Maeda, M. Higasa, and K. Kashima, "In-situ observation of bubble formation at silicon melt–silica glass interface," J. Cryst. Growth **318**(1), 196–199 (2011).
11. S. M. Schnurre and R. Schmid-Fetzer, "Reactions at the liquid silicon/silica glass interface," J. Cryst. Growth **250**(3-4), 370–381 (2003).
12. J. Ballato, T. Hawkins, P. Foy, B. Yazgan-Kokuoz, C. McMillen, L. Burka, S. Morris, R. Stolen, and R. Rice, "Advancements in semiconductor core optical fiber," Opt. Fiber Technol. **16**(6), 399–408 (2010).
13. S. Morris, T. Hawkins, P. Foy, C. McMillen, J. Fan, L. Zhu, R. Stolen, R. Rice, and J. Ballato, "Reactive molten core fabrication of silicon optical fiber," Opt. Mater. Express **1**(6), 1141–1149 (2011).
14. S. Morris, T. Hawkins, P. Foy, J. Hudson, L. Zhu, R. Stolen, R. Rice, and J. Ballato, "On loss in silicon core optical fibers," Opt. Mater. Express **2**(11), 1511–1519 (2012).
15. K. Wilm and G. Frischat, "Coating and diffusion studies to improve the performance of silica glass crucibles for the preparation of semiconducting silicon single crystals," Glass Technol. - Eur. J. Glass Sci. Technol. A **47**(1), 7–14 (2006).
16. A. Cröll, R. Lantzsch, S. Kitanov, N. Salk, F. R. Szofran, and A. Tegetmeier, "Melt-crucible wetting behavior in semiconductor melt growth systems," Cryst. Res. Technol. **38**(78), 669–675 (2003).
17. I. Brynjulfsen, A. Bakken, M. Tangstad, and L. Arnberg, "Influence of oxidation on the wetting behavior of liquid silicon on Si_3N_4-coated substrates," J. Cryst. Growth **312**(16-17), 2404–2410 (2010).

#187147 - $15.00 USD Received 15 Mar 2013; revised 16 Apr 2013; accepted 17 Apr 2013; published 23 Apr 2013

18. F. A. Martinsen, E. F. Nordstrand, and U. J. Gibson, "Purification of melt-spun metallurgical grade silicon micro-flakes through a multi-step segregation procedure," J. Cryst. Growth **363**, 33–39 (2013).
19. F. He, S. Zheng, and C. Chen, "The effect of calcium oxide addition on the removal of metal impurities from metallurgical-grade silicon by acid leaching," Metall. Mater. Trans., B, Process Metall. Mater. Proc. Sci. **43**(5), 1011–1018 (2012).
20. M. D. Himel and U. J. Gibson, "Measurement of planar waveguide losses using a coherent fiber bundle," Appl. Opt. **25**(23), 4413–4416 (1986).
21. M. H. Jenkins, B. S. Phillips, Y. Zhao, M. R. Holmes, H. Schmidt, and A. R. Hawkins, "Optical characterization of optofluidic waveguides using scattered light imaging," Opt. Commun. **284**(16-17), 3980–3982 (2011).
22. Lambda-Photometrics, "Model2010" http://www.lambdaphoto.co.uk/products/150.110.100.007 (2013).
23. C. W. Bale, P. Chartrand, S. A. Degterov, G. Eriksson, K. Hack, R. Ben Mahfoud, J. Melançon, A. D. Pelton, and S. Petersen, "FactSage thermochemical software and database," Calphad **26**(2), 189–228 (2002).
24. A. Cruz-Ramírez, J. Romo-Castañeda, M. Á. Hernández-Pérez, M. Vargas-Ramírez, A. Romero-Serrano, and M. Hallen-López, "An application of infrared analysis to determine the mineralogical phases formation in fluxes for thin slab casting of steel," J. Fluor. Chem. **132**(5), 323–326 (2011).
25. X. Huang, S. Koh, K. Wu, M. Chen, T. Hoshikawa, K. Hoshikawa, and S. Uda, "Reaction at the interface between Si melt and a Ba-doped silica crucible," J. Cryst. Growth **277**(1-4), 154–161 (2005).
26. D. Romero, J. M. F. Romero, and J. J. Romero, "Distribution of metal impurities in silicon wafers using imaging-mode multi-elemental laser-induced breakdown spectrometry," J. Anal. At. Spectrom. **14**(2), 199–204 (1999).
27. A. J. Eraker and U. J. Gibson (Dept. of Physics, Norwegian Univ. of Sci. and Technol., 7491 Trondheim, Norway) are preparing a manuscript to be called "Optical loss measurements in silicon fibers".

1. Introduction

Fiber materials for the infrared are of increasing importance as new laser sources are developed throughout the region from 1 to 10 microns. Although there has been significant development of glassy materials [1,2], silicon-core fibers have attracted particular interest due to their high index of refraction, non-linear properties [3], and potential as all-optical light modulators [4]. High-quality fibers of limited length have been fabricated by chemical vapour deposition within the pores of photonic crystal optical fibers [5].

Recently, Scott [6] and Ballato [7] published results on the use of molten core fiber-optic pulling techniques to form silicon and germanium [8] fibers encased in glass. This technique offers the promise of scale-up to industrial quantities of material. While production of many meters of germanium fiber with core diameters down to 15 microns [8] is reported, silicon fibers drawn in a fiber tower have been larger, with core diameters of 100 microns [7] and shorter. Benchtop fibers of silicon with cores down to 10 microns have been demonstrated using a powder-in tube method [6], but lengths have been limited to a few cm [9]. Gas production due to the reaction of silicon with silicon oxide [10], stress due to thermal mismatch with the glass sheath [11], and discontinuous cores can all contribute to poor performance. Significant progress has been made in assessing and improving the crystallographic quality [12] and impurity content [13] of these fibers, and in understanding the mechanisms responsible for optical losses [14].

One aspect that has so far not been investigated is the use of an intermediate layer between the silicon and the silica tube to moderate stress, remove impurities and provide a gradient index of refraction. Although there are some wetting studies of molten silicon available, they center around materials suitable as crucibles for melting [15] and directional recrystallization [16,17]. Recent studies on the use of silicon carbide for removal of oxygen [13], and purification of silicon in low-dimensional structures [18] suggested the use of a reactive species for this purpose. Choice of a suitable interface material was guided by the principles that it should be an oxide to minimize chemical complexity, it should form a eutectic with the silicon with a melting point below the softening point of the glass to reduce stress, and that the metal ion should be less electronegative than silicon to assist with oxygen scavenging from the core. Alkaline earth oxides are routinely used in the purification of silicon [19], and calcium oxide satisfies the criteria above. CaO forms hydroxides upon the addition of water, and thus an aqueous route can be used in the preparation of a preform with a layer of CaO on the inside of the silica. NaO, BaO, MgO and SrO were also investigated, with varying degrees of success; SrO and NaO, as well as NaO-BaO mixtures were least successful, resulting in

#187147 - $15.00 USD Received 15 Mar 2013; revised 16 Apr 2013; accepted 17 Apr 2013; published 23 Apr 2013

distortion of the glass-silicon interface, or large cavities in the core. CaO and CaO-MgO blends performed best, and the results presented here are on CaO. Several grades of silicon were used in these studies, as we also have interest in the segregation of impurities in limited-dimension samples [18], but the results here are limited to electronic and solar grades. In these preliminary studies, the emphasis was on the mechanical and microstructural properties. Use of higher purity starting materials can be expected to improve the optical properties of the fibers.

We present studies on the use of alkaline-earth interface modifiers to improve the mechanical properties of silicon-based fibers, demonstrating low-oxygen core content, core diameters down to 10 microns and low damage to the silica cladding, as evidenced by small bending radii. This technique should be adaptable to the production of high quality optical fibers when performed in a commercial drawing tower, particularly when employing MOCVD-deposited oxide interface modifiers.

2. Experimental

We prepared preforms using small diameter silica tubes (i.d. 2 mm, o.d. 4mm), with a typical length of 200mm. The ratio of the core to cladding dimensions is large, and the silica cladding of fibers prepared without the interface modifier were stressed and cracked so extensively that they disintegrated on handling, or in some cases spontaneously upon cooling.

Deionized water and CaO powder (Sigma Aldrich >99.9%) were combined in a 3:1 ratio a beaker and allowed to react, forming “milk of lime” according to the reaction

$$CaO(s) + H_2O \rightarrow Ca(OH)_2(aq) \quad (1)$$

The preform tube was connected to a low-level vacuum, and the hydroxide mixture was drawn into the tube by briefly inserting the end of the tube into the liquid. This allowed us to make uniformly coated tubes, where the thickness of the coating was regulated by the viscosity of the hydroxide mix. Typical ratios of oxide to silicon were 1:8 by weight. The tubes were dried overnight at 100 °C before sealing one end using an oxy-acetylene torch. The baking dehydrates the coating and returns it to the oxide form, though reaction with atmospheric CO_2 may result in small quantities of calcium carbonate. Any carbonate would be decomposed at 825 °C, well below the temperature at which fiber drawing occurs. Silicon granules were prepared by crushing polysilicon or an n-type solar silicon wafer (Norsun, nominal 7N purity base material) in a mortar and pestle to a size of approximately 0.5 mm or less. The coated preform was then filled with this powder.

The preforms were held vertically, and heated using an oxyacetylene flame centered above the bottom of the preform until melting of the silicon was observed. Further heating was applied to soften the silica. The high temperature flame precluded measurement of the draw temperature. The bottom of the tube was then pulled down at speeds of 60-150 meters per minute, resulting in fibers of up to 450 mm in length, limited by the vertical clearance of our setup. Fibers drawn with or without vacuum application during the pull showed no significant differences, and results presented here are for fibers drawn in air.

Analysis of the fibers was performed using x-ray fluorescence microprobe with wavelength and energy dispersive spectrometers, scanning electron microscopy, Raman spectroscopy (Horiba LabRam HR800-UV) and UV photoluminescence spectroscopy. An excimer laser operating at 248 nm was used as the UV excitation source, and an Avantis Avaspec ULS2048 spectrometer was used to acquire the optical data. Cross-sectional samples were prepared by mechanical polishing; these were used for microprobe and Raman characterization.

Optical waveguide loss measurements were made by collecting the scattered light as a function of distance along the bare silicon core [20–22]. The scatter method allowed us to make measurements insensitive to variations in the input coupling. We used a modulated 5 mW fiber-coupled laser diode operating at 1.55 microns, an amplified Ge detector (ThorLabs

#187147 - $15.00 USD Received 15 Mar 2013; revised 16 Apr 2013; accepted 17 Apr 2013; published 23 Apr 2013

PDA30B) and a lock-in amplifier. For most measurements, the silicon fiber was mounted inside a commercial fiber optic ferrule, and a ferrule coupler then aligned it with the output fiber of the laser. The silica and CaO were removed by HF etching prior to measurements, to eliminate cladding modes, and a pickup fiber was scanned along the waveguide to collect the scattered light for a determination of the fiber losses. Figure 1 shows this setup. Measurements made with a GRIN lens collimator and a 10x objective mounted in an x-y translator for coupling into the fiber yielded similar results.

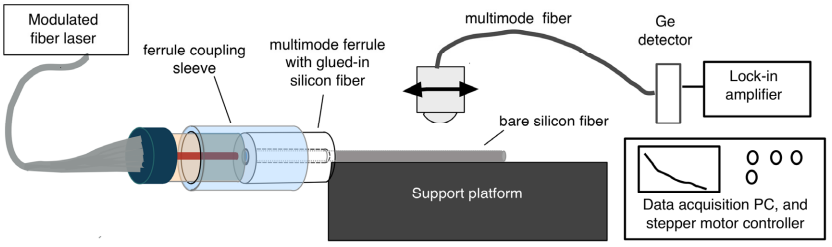

Fig. 1. Schematic of butt-coupling and scanning fiber arrangement.

Multiple measurements of an individual fiber are highly reproducible (e.g. with 10 measurements, the mean loss was 4.365 with a standard deviation of 0.0243 and a coefficient of determination (R^2) of >.972 for all the fitted curves). Intentionally tilting the fiber scanning stage by 1 degree or defocussing the pickup lens by 60% percent of its focal length resulted in less than 5% change in the fitted value. Rotating the fiber around its axis did not lead to a measurable change in the derived loss value.

Scanning electron microscopy of the fiber surface after etching was performed in a Hitachi TM-3000 tabletop SEM.

3. Results and discussion

Figure 2(a) shows a scanning electron micrograph of the cross-section of one of the fibers drawn from metallurgical grade silicon using CaO as an interface modifier, Fig. 2(b) is a microprobe scan across the interface from top to bottom, and Fig. 2(c) is a Raman spectrum from the core.

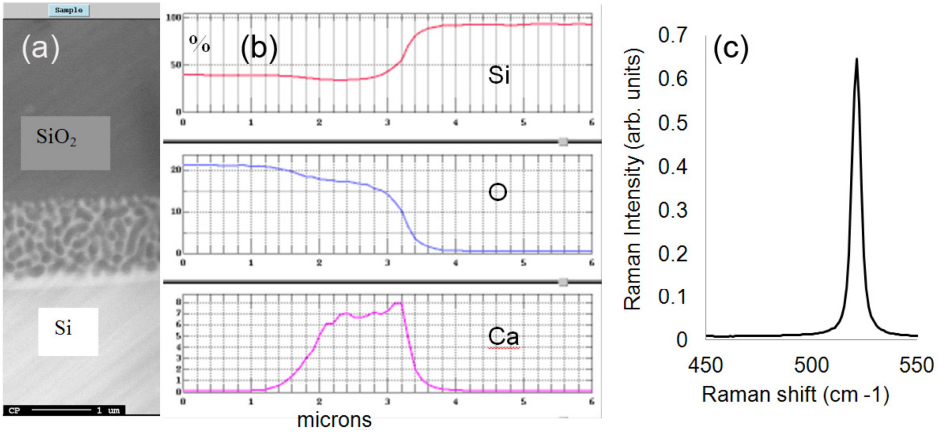

Fig. 2. (a) SEM image (scale bar is 1µm) (b) microprobe data from a line scan from the cladding to the core. The interface modifier makes a layer about one micron thick, with good confinement of calcium to the layer. Oxygen in the silicon core is at the limit of detection. (c) Si Raman signal from a fiber core.

Although the absolute percentages of the components have not been calibrated for the microprobe data on this system, the relative amounts can be used to interpret the results.

#187147 - $15.00 USD Received 15 Mar 2013; revised 16 Apr 2013; accepted 17 Apr 2013; published 23 Apr 2013

The calcium is localized at the interface, the silicon content tapers off as the eutectic microstructure takes over. There is a small drop in the silicon content in the interface region, relative to the amount in the silica cladding; this correlates with the presence of Ca. The oxygen content is reduced in the interface region, showing that the region is a mixture of semiconductor and oxide; this demonstrates that the index of refraction of this region will be intermediate between that of the core and cladding. The oxygen content in the silicon core is at the detection limit of the technique. This is in contrast to the initial results of Ballato et al [7], and comparable to the results that they achieved with silicon carbide used to scavenge oxygen [13]. The 100-300 nm grain size of the eutectic microstructure is typical for this composition and drawing condition, and represents a potential challenge for transmission of short wavelengths as it may introduce scatter. In the 3-5 micron region where these fibers might be most useful, this will be less problematic. Preliminary results on binary mixtures of alkaline earth oxides (MgOH and CaO) suggest that this structure is finer the presence of an additional oxide, most likely due to increased nucleation, as the MgO-rich phases will precipitate out at higher temperatures, seeding the solidification of the Ca-rich phase. The Raman results in Fig. 2(c), with a strong peak at 520 cm^{-1}, and no signal at 480 cm^{-1} demonstrate that the core is crystalline silicon, with little or no amorphous component.

Figure 3 shows the phase diagram for CaO-SiO_2 [23]. We believe that the eutectic present at 1437 °C is responsible for the superior drawing properties of fibers made with this interface

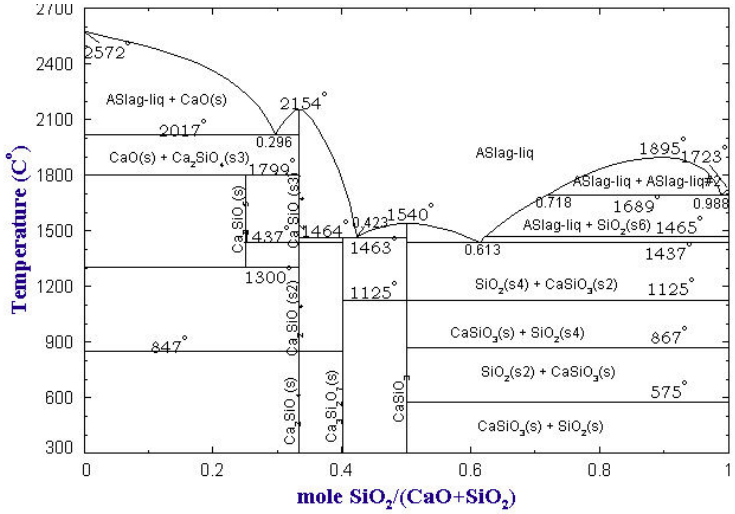

Fig. 3. Phase diagram of the CaO – SiO_2 system [23].

modifier. A lower-viscosity liquid forms at the interface between the silica glass and the molten silicon, allowing differential contraction. The silicon and the silicate phase separate, and we have not observed silicate inclusions in the fiber core with CaO, even when starting with a mixture of silicon and CaO powders. This suggests that the silicates preferentially wet the preform walls. Although the eutectic forms at a temperature slightly above the silicon melting point in the pure oxide system, it is likely that this temperature is suppressed in the presence of liquid silicon. The oxides are expected to separate into a mixture of wollastonite ($CaSiO_3$) and SiO_2 upon cooling. Wollastonite is a byproduct in silicon slag refining, and is used as a flux for low-temperature steel manufacturing [24]. It is known to be an effective sink for impurities in silicon, and the lower electronegativity of calcium relative to silicon explains the oxygen scavenging that we observe. Related studies on silica crucibles coated with BaO decreased erosion of the silica glass by molten silicon, in the presence of the coating, although there are conflicting interpretations of the mechanism [15,25].

#187147 - $15.00 USD Received 15 Mar 2013; revised 16 Apr 2013; accepted 17 Apr 2013; published 23 Apr 2013

Figure 4(a) presents an SEM image, showing the small core sizes possible. This fiber end was fractured, and shows damage due to that process. Figure 4(b) shows the bending radius

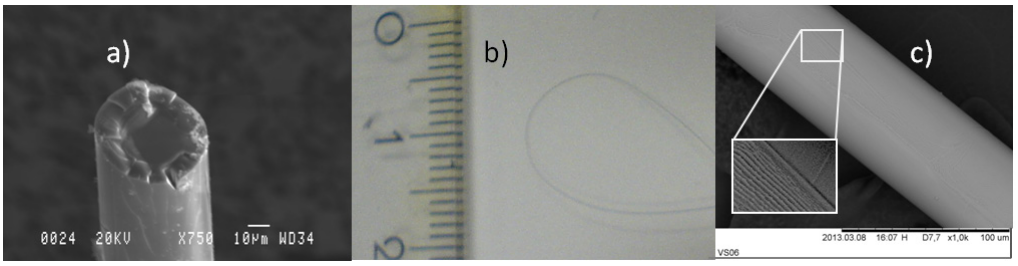

Fig. 4. (a) Fractured small-diameter fiber, (b) bending radius of the fiber shown in the first panel (ruled markings are cm) (c) SEM image of the surface of a ~65 µm diameter fiber, used for waveguide loss measurements, after removal of the glass coating. Striations shown in the expanded and contrast-enhanced inset likely arise from the eutectic decomposition of the oxides.

achieved with small fibers, and Fig. 4(c) shows a bare silicon core; close inspection shows striations with a periodicity of ~100nm along the surface.

Shown in Fig. 5 are fluorescence results obtained with excitation at 248nm for a bare silica tube, calcium oxide powder, and fibers prepared with CaO at the interface. The bulk of the emission is due to the silica cladding, but peaks that are not accounted for by either the silica cladding or CaO appear at 300 and 670 nm.

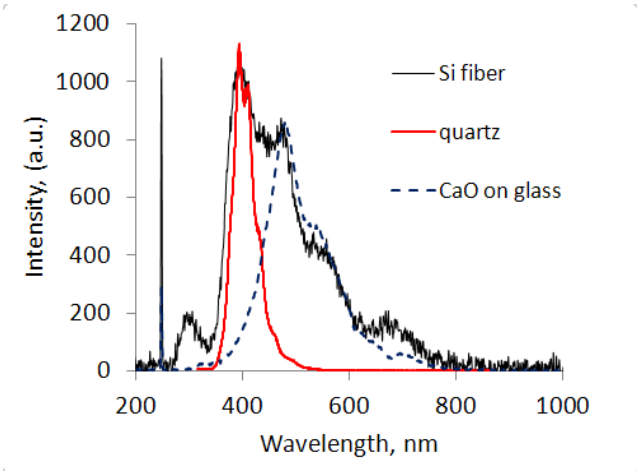

Fig. 5. Fluorescence spectrum of fibers, empty silica tubing, and CaO slurry after drying.

The shoulder at 500 nm is thought to be calcium carbonate, and the peak at 300 is due to silicon [26]. Calcium silicate is not expected to fluoresce in the visible, except in the presence of impurities. As the purity of our calcium oxide powder was only 99.9%, the peak at 670 is likely due to impurity inclusion in the nanocrystalline host in configurations that allow optical emission. It is also possible that impurities removed from the silicon melt contribute to this signal.

Measured losses on bare silicon fiber cores from different preforms varied from 3.8dB/cm to over 20dB/cm, depending on the surface quality of the fiber (which is a function of the interface layer thickness and drawing parameters), and the type of silicon used. The sample shown in Fig. 4(c), made from the Norsun material, had losses of approximately 3.8dB/cm, measured over a 1 cm length; all fibers from this material had losses less than or equal to 11dB/cm; secondary ion mass spectroscopy will be performed [27] to determine the impurity levels in the different silicon materials. However, loss measurements were influenced by areas with high scatter; in fibers with higher losses, the scatter could be correlated with core-surface

#187147 - $15.00 USD Received 15 Mar 2013; revised 16 Apr 2013; accepted 17 Apr 2013; published 23 Apr 2013

features observed in the microscope. Thicker interface layers appeared to be associated with hydrodynamic instabilities that were responsible for the surface roughness of the cores. Measurements of the throughput yielded comparable values for the loss, despite poor end face quality, which leads us to believe that reduced losses will be observed in smoother fibers, and those dominated by lower order modes, where the field is more confined to the core.

4. Conclusions

We demonstrate the ability to pull small diameter silicon fibers with good flexibility when using an interface modifier to scavenge oxygen from the core, relieve thermal mismatch, and decrease the viscosity of the boundary between the molten silicon and the silica glass. Alkaline earth oxides, particularly CaO and MgO lead to formation of fibers with reduced core voids, high quality interfaces and superior mechanical properties. Introduction of interface modifiers in preforms made by MOCVD, and the use of a commercial drawing tower may be expected to result in material with improved uniformity and lower losses.

Acknowledgments

We are grateful for support from the Norwegian University of Science and Technology, the Norwegian Discovery fund, and X. D. Yang, Fredrik Martinson, and Andrey Volyakin for assistance with analytical measurements.

#187147 - $15.00 USD Received 15 Mar 2013; revised 16 Apr 2013; accepted 17 Apr 2013; published 23 Apr 2013

Bibliography

[1] F. Seitz and N.G. Einspruch. *Electronic genie: the tangled history of silicon.* University of Illinois Press, 1998. ISBN 9780252023835.

[2] K.C. Kao and G.A. Hockham. Dielectric-fibre surface waveguides for optical frequencies. *Optoelectronics, IEE Proceedings J*, 133(3):191–198, 1986. ISSN 0267-3932.

[3] N. Takeda. Spherical silicon 1 mm device and its clustering. In *Advanced Packaging Materials: Processes, Properties and Interfaces, 2001. Proceedings. International Symposium on*, pages 86–91, 2001.

[4] Anna Peacock and Noel Healy. Parabolic pulse generation in tapered silicon fibers. *Opt. Lett.*, 35(11):1780–1782, Jun 2010. doi: 10.1364/OL.35.001780.

[5] Kyle Preston, Sasikanth Manipatruni, Alexander Gondarenko, Carl B. Poitras, and Michal Lipson. Deposited silicon high-speed integratedelectro-optic modulator. *Opt. Express*, 17(7):5118–5124, Mar 2009. doi: 10.1364/OE.17.005118.

[6] D. Kouznetsov and J.V. Moloney. Highly efficient, high-gain, short-length, and power-scalable incoherent diode slab-pumped fiber amplifier/laser. *Quantum Electronics, IEEE Journal of*, 39(11):1452–1461, 2003. ISSN 0018-9197. doi: 10.1109/JQE.2003.818311.

[7] B. Cowan. Optical damage threshold of silicon for ultrafast infrared pulses. *AIP Conference Proceedings*, 877(1):837–843, 2006. doi: 10.1063/1.2409223.

[8] Xiushan Zhu and N Peyghambarian. High-power zblan glass fiber lasers: review and prospect. *Advances in OptoElectronics*, 2010, 2010.

[9] J. Ballato, T. Hawkins, P. Foy, B. Yazgan-Kokuoz, C. McMillen, L. Burka, S. Morris, R. Stolen, and R. Rice. Advancements in semiconductor core

optical fiber. *Optical Fiber Technology*, 16(6):399 – 408, 2010. ISSN 1068-5200. doi: 10.1016/j.yofte.2010.08.006. ¡ce:title¿Special Fiber Structures and their Applications¡/ce:title¿.

[10] Noel Healy, Laura Lagonigro, Justin R. Sparks, Stuart Boden, Pier J. A. Sazio, John V. Badding, and Anna C. Peacock. Polycrystalline silicon optical fibers with atomically smooth surfaces. *Opt. Lett.*, 36(13):2480–2482, Jul 2011. doi: 10.1364/OL.36.002480.

[11] Pier J. A. Sazio, Adrian Amezcua-Correa, Chris E. Finlayson, John R. Hayes, Thomas J. Scheidemantel, Neil F. Baril, Bryan R. Jackson, Dong-Jin Won, Feng Zhang, Elena R. Margine, Venkatraman Gopalan, Vincent H. Crespi, and John V. Badding. Microstructured optical fibers as high-pressure microfluidic reactors. *Science*, 311(5767):1583–1586, 2006. doi: 10.1126/science.1124281.

[12] Ursula Gibson. Alkaline oxide modifiers for the production of semiconductor fibers. In *Workshop on Specialty Optical Fibers and their Applications*, 2013.

[13] J. Ballato, T. Hawkins, P. Foy, R. Stolen, B. Kokuoz, M. Ellison, C. McMillen, J. Reppert, A. M. Rao, M. Daw, S. R. Sharma, R. Shori, O. Stafsudd, R. R. Rice, and D. R. Powers. Silicon optical fiber. *Opt. Express*, 16(23):18675–18683, Nov 2008. doi: 10.1364/OE.16.018675.

[14] S.M Schnurre and R Schmid-Fetzer. Reactions at the liquid silicon/silica glass interface. *Journal of Crystal Growth*, 250(34):370 – 381, 2003. ISSN 0022-0248. doi: 10.1016/S0022-0248(02)02491-0.

[15] Jing CAI, Xue tao LUO, Cheng hao LU, Geir Martin Haarberg, Annabelle Laurent, Ole Edvard Kongstein, and Shu lan Wang. Purification of metallurgical grade silicon by electrorefining in molten salts. *Transactions of Nonferrous Metals Society of China*, 22(12):3103 – 3107, 2012. ISSN 1003-6326. doi: 10.1016/S1003-6326(11)61577-X.

[16] P. Mishra, A. Chakraverty, and H.D. Banerjee. Production and purification of silicon by calcium reduction of rice-husk white ash. *Journal of Materials Science*, 20(12):4387–4391, 1985. ISSN 0022-2461. doi: 10.1007/BF00559326.

[17] Patent, Anton More et. al.,US 4151264 A, 1979, 1979.

[18] D.K. Mynbaev and L.L. Scheeiner. *Fiber Optic Communications Technology*. Prentice Hall PTR, 2001. ISBN 9780139620690.

[19] M. Gregory Forest and Hong Zhou. Unsteady analyses of thermal glass fibre drawing processes. *Euro. J. Appl. Math*, pages 479–496, 2001.

[20] Meng-Lun Hsueh, Bing-Yuh Lu, Fok-Ching Chong, and Sham-Tsong Shiue. Design of double-coated optical fibers to minimize microbending losses caused by hydrostatic-pressure-induced creep deformation of polymeric coatings. *Optical Engineering*, 49(6):065006–065006–5, 2010. doi: 10.1117/1.3454386.

[21] John A. Jay. An overview of macrobending and microbending of optical fibers. Electronic, December 2010. URL `www.corning.com/assets/0/433/573/637/639/1BEA48AC-D675-44C7-AA18-11A3A1A0ADBD.pdf`.

[22] J.M. Senior. *Optical fiber communications: principles and practice*. Prentice-Hall international series in optoelectronics. Prentice Hall, 1992. ISBN 9780136354260.

[23] M. Ohashi, K. Shiraki, and K. Tajima. Optical loss property of silica-based single-mode fibers. *Lightwave Technology, Journal of*, 10(5):539–543, 1992. ISSN 0733-8724. doi: 10.1109/50.136085.

[24] G. Keiser. *Optical Fiber Communications*. McGraw-Hill Education (India) Pvt Limited, 2008. ISBN 9780070648104.

[25] C. McMillen, G. Brambilla, S. Morris, T. Hawkins, P. Foy, N. Broderick, E. Koukharenko, R. Rice, and J. Ballato. On crystallographic orientation in crystal core optical fibers ii: Effects of tapering. *Optical Materials*, 35(2):93 – 96, 2012. ISSN 0925-3467. doi: http://dx.doi.org/10.1016/j.optmat.2012.06.020.

[26] Brian Scott, Ke Wang, Vincent Caluori, and Gary Pickrell. Fabrication of silicon optical fiber. *Optical Engineering*, 48(10):100501–100501–3, 2009. doi: 10.1117/1.3250189.

[27] Yuzuru Sato, Yuichi Kameda, Toru Nagasawa, Takashi Sakamoto, Shinpei Moriguchi, Tsutomu Yamamura, and Yoshio Waseda. Viscosity of molten silicon and the factors affecting measurement. *Journal of Crystal Growth*, 249 (34):404 – 415, 2003. ISSN 0022-0248. doi: 10.1016/S0022-0248(02)02153-X.

[28] T.F. Ciszek. Silicon shot solidification in water. *Journal of Crystal Growth*, 310(79):2198 – 2203, 2008. ISSN 0022-0248. doi: 10.1016/j.jcrysgro.2007.11.051. ¡ce:title¿the Proceedings of the 15th International Conference on Crystal Growth (ICCG-15) in conjunction with the International Conference on Vapor

Growth and Epitaxy and the {US} Biennial Workshop on Organometallic Vapor Phase Epitaxy¡/ce:title¿.

[29] W.N. Sharpe, Kamili M. Jackson, K.J. Hemker, and Z. Xie. Effect of specimen size on young's modulus and fracture strength of polysilicon. *Microelectromechanical Systems, Journal of*, 10(3):317–326, 2001. ISSN 1057-7157. doi: 10.1109/84.946774.

[30] Stephanie Morris, Colin McMillen, Thomas Hawkins, Paul Foy, Roger Stolen, John Ballato, and Robert Rice. The influence of core geometry on the crystallography of silicon optical fiber. *Journal of Crystal Growth*, 352(1):53 – 58, 2012. ISSN 0022-0248. doi: 10.1016/j.jcrysgro.2011.12.009. ¡ce:title¿The Proceedings of the 18th American Conference on Crystal Growth and Epitaxy¡/ce:title¿.

[31] R. Hull and INSPEC (Information Service). *Properties of Crystalline Silicon*. EMIS datareviews series. INSPEC, The Institution of Electrical Engineers, 1999. ISBN 9780852969335.

[32] H. L. Watson. Some properties of fused quartz and other forms of silicondioxide1. *Journal of the American Ceramic Society*, 9(8):511–534, 1926. ISSN 1551-2916.

[33] A. A. Griffith. The phenomena of rupture and flow in solids. *Philosophical Transactions of the Royal Society of London. Series A, Containing Papers of a Mathematical or Physical Character*, 221:pp. 163–198, 1921. ISSN 02643952.

[34] S.M Schnurre and R Schmid-Fetzer. Reactions at the liquid silicon/silica glass interface. *Journal of Crystal Growth*, 250(34):370 – 381, 2003. ISSN 0022-0248. doi: 10.1016/S0022-0248(02)02491-0.

[35] Martin A. Green. Self-consistent optical parameters of intrinsic silicon at 300k including temperature coefficients. *Solar Energy Materials and Solar Cells*, 92(11):1305 – 1310, 2008. ISSN 0927-0248. doi: 10.1016/j.solmat.2008.06.009.

[36] Rei Kitamura, Laurent Pilon, and Miroslaw Jonasz. Optical constants of silica glass from extreme ultraviolet to far infrared at near room temperature. *Appl. Opt.*, 46(33):8118–8133, Nov 2007. doi: 10.1364/AO.46.008118.

[37] D.R. Lide. *CRC Handbook of Chemistry and Physics 2004-2005: A Ready-Reference Book of Chemical and Physical Data*. CRC Handbook of Chemistry and Physics, 93rd Ed. CRC PressI Llc, 2012. ISBN 9780849304859.

[38] H. Fredriksson and U. Akerlind. *Solidification and Crystallization Processing in Metals and Alloys*. Wiley, 2012. ISBN 9781119993056.

[39] Sumanth Shankar. *Casting*, volume 15. ASM International, 2008.

[40] P. J. Anderson and R. F. Horlock. Thermal decomposition of magnesium hydroxide. *Trans. Faraday Soc.*, 58:1993–2004, 1962. doi: 10.1039/TF9625801993.

[41] P. E. Halstead and A. E. Moore. 769. the thermal dissociation of calcium hydroxide. *J. Chem. Soc.*, 0:3873–3875, 1957. doi: 10.1039/JR9570003873.

[42] G. Brauer. *Handbook of preparative inorganic chemistry*. Number v. 1 in Handbook of Preparative Inorganic Chemistry. Academic Press, 1963.

[43] Bengt Hallstedt. Thermodynamic calculation of some subsystems of the al-ca-mg-si-o system. *Journal of phase equilibria*, 14(6):662–675, 1993.

[44] S. A. Degterov G. Eriksson K. Hack R. Ben Mahfoud J. Melanon A. D. Pelton C. W. Bale, P. Chartrand and S. Petersen. Factsage thermochemical software and database. 26(2):189228, 2002.

[45] A. Romero-Serrano, A. Cruz-Ramirez, B. Zeifert, M. Hallen-Lopez, and A. Hernandez-Ramirez. Thermodynamic modeling of the bao-sio2 and sro-sio2 binary melts. *Glass Physics and Chemistry*, 36(2):171–178, 2010. ISSN 1087-6596. doi: 10.1134/S1087659610020045.

[46] K. J. Hubbard and D. G. Schlom. Thermodynamic stability of binary oxides in contact with silicon. *Journal of Materials Research*, 11:2757–2776, 10 1996. ISSN 2044-5326. doi: 10.1557/JMR.1996.0350.

[47] Haojie Yuan and R Stanley Williams. Solid-phase equilibria for metal-silicon-oxygen ternary systems. 1. magnesium, calcium, strontium and barium. *Chemistry of Materials*, 2(6):695–700, 1990.

[48] M.H. Reeve. Optical fibre cables. *Radio and Electronic Engineer*, 51(7.8): 327–332, 1981. ISSN 0033-7722. doi: 10.1049/ree.1981.0050.

[49] J. Goldstein. *Scanning Electron Microscopy and X-Ray Microanalysis*. Kluwer Academic/Plenum Publishers, 2003. ISBN 9780306472923.

[50] R.F. Egerton. *Physical Principles of Electron Microscopy: An Introduction to TEM, SEM, and AEM*. Springer, 2005. ISBN 9780387258003.

[51] F. Giessibl. Advances in atomic force microscopy. *Reviews of Modern Physics*, 75:949–983, July 2003. doi: 10.1103/RevModPhys.75.949.

[52] Nader Jalili and Karthik Laxminarayana. A review of atomic force microscopy imaging systems: application to molecular metrology and biological sciences. *Mechatronics*, 14(8):907 – 945, 2004. ISSN 0957-4158. doi: http://dx.doi.org/10.1016/j.mechatronics.2004.04.005.

[53] B.L. Scott, Ke Wang, and G. Pickrell. Fabrication of n-type silicon optical fibers. *Photonics Technology Letters, IEEE*, 21(24):1798–1800, 2009. ISSN 1041-1135. doi: 10.1109/LPT.2009.2033388.

[54] Won-Kyu Rhim and Kenichi Ohsaka. Thermophysical properties measurement of molten silicon by high-temperature electrostatic levitator: density, volume expansion, specific heat capacity, emissivity, surface tension and viscosity. *Journal of Crystal Growth*, 208(14):313 – 321, 2000. ISSN 0022-0248. doi: 10.1016/S0022-0248(99)00437-6.

[55] T Zhang, S Shang, F Yin, A Aishah, A Salmiah, and T.L Ooi. Adsorptive behavior of surfactants on surface of portland cement. *Cement and Concrete Research*, 31(7):1009 – 1015, 2001. ISSN 0008-8846. doi: http://dx.doi.org/10.1016/S0008-8846(01)00511-7.

[56] L.L. Tedder, G. Lu, and J.E. Crowell. Mechanistic studies of dielectric thin film growth by low pressure chemical vapor deposition: The reaction of tetraethoxysilane with sio2 surfaces. *Journal of Applied Physics*, 69(10): 7037–7049, 1991. cited By (since 1996)39.

[57] Lutz Rsch, Peter John, and Rudolf Reitmeier. *Silicon Compounds, Organic.*

[58] S. Nakamura and T. Hibiya. Thermophysical properties data on molten semiconductors. *International Journal of Thermophysics*, 13(6):1061–1084, 1992. ISSN 0195-928X. doi: 10.1007/BF01141216.

[59] Liqun Zhang, James A. Van Orman, and Daniel J. Lacks. Molecular dynamics investigation of mgocaosio2 liquids: Influence of pressure and composition on density and transport properties. *Chemical Geology*, 275 (12):50 – 57, 2010. ISSN 0009-2541. doi: http://dx.doi.org/10.1016/j.chemgeo.2010.04.012. URL `http://www.sciencedirect.com/science/article/pii/S0009254110001476`.

[60] E. Bartholom. *Z, Electrochem.*, 54:169, 1950.

[61] N. Healy, J. R. Sparks, M. N. Petrovich, P. J. A. Sazio, J. V. Badding, and A. C. Peacock. Large mode area silicon microstructured fiber with robust dual mode guidance. *Opt. Express*, 17(20):18076–18082, Sep 2009. doi: 10.1364/OE.17.018076.

[62] Erlend F. Nordstrand, Andrew N. Dibbs, Andreas J. Eraker, and Ursula J. Gibson. Alkaline oxide interface modifiers for silicon fiber production. *Opt. Mater. Express*, 3(5):651–657, May 2013. doi: 10.1364/OME.3.000651.

[63] A. J. Eraker. Loss measurements in silicon core optical fibers. Master's thesis, Norwegian University of Science and Technology, 2013.

[64] Laura Lagonigro, Noel Healy, Justin R. Sparks, Neil F. Baril, Pier J. A. Sazio, John V. Badding, and Anna C. Peacock. Low loss silicon fibers for photonics applications. *Applied Physics Letters*, 96(4):041105, 2010. doi: 10.1063/1.3294630.

[65] J.W. Anthony, R.A. Bideaux, K.W. Bladh, and M.C. Nichols. *Handbook of mineralogy*. Number v. 2 in Handbook of Mineralogy. Mineral Data Publishing, 1995. ISBN 9780962209710.

[66] M. Weizman, C. Klimm, N.H. Nickel, and B. Rech. Origin of preferential grain orientation in excimer laser-induced crystallization of silicon thin films. *Applied Physics Letters*, 100(16), 2012. cited By (since 1996)2.